AD-A050 696 APPLIED THEORY INC LOS ANGELES CALIF F/G 18/3
LIMITATIONS ON THE SIZE OF EJECTA CRATERS.(U)
NOV 75 J G TRULIO, N K PERL, R W LATHAM DNA001-75-C-0298
UNCLASSIFIED ATR-75-44-1 DNA-4253F NL

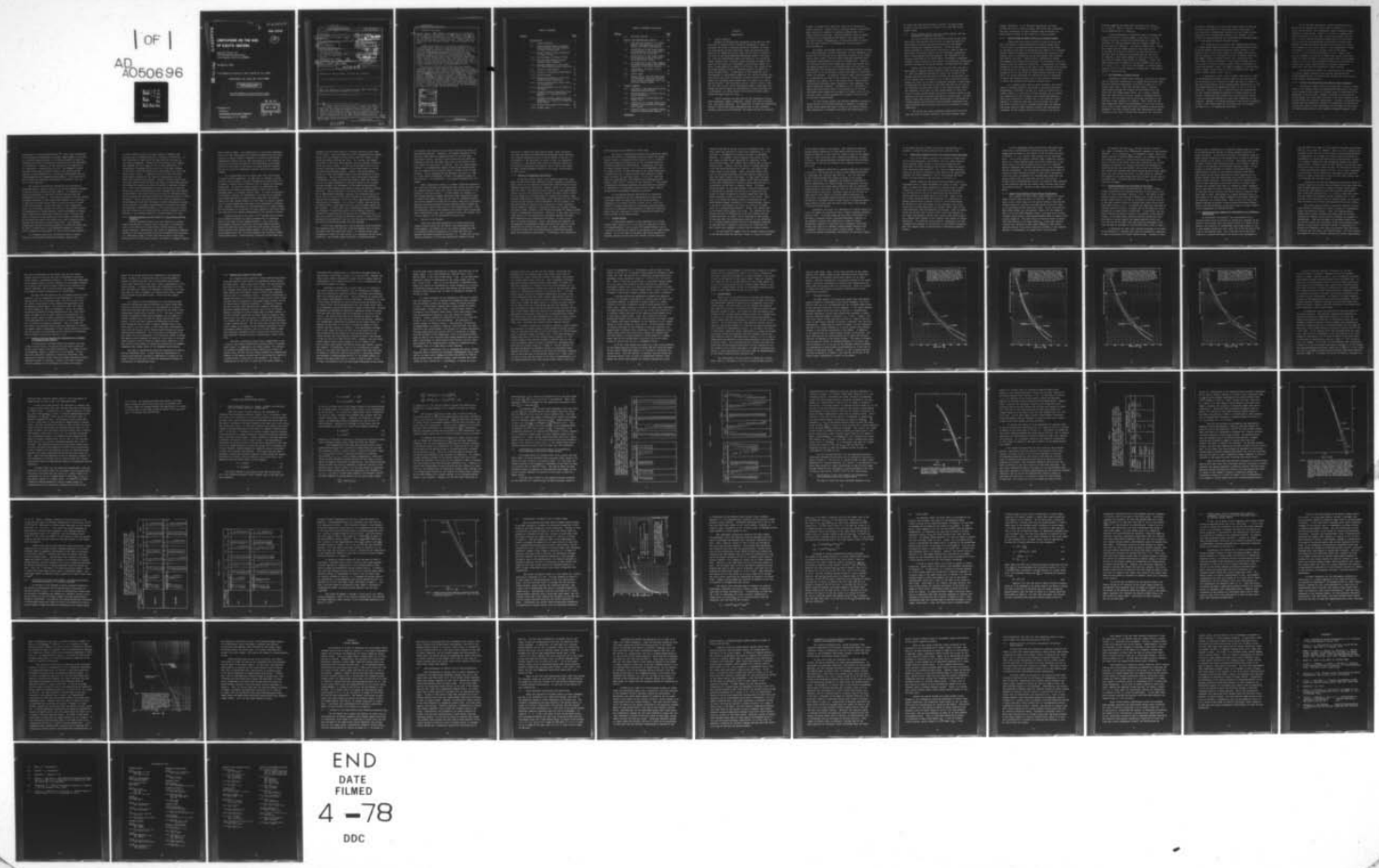

END
DATE FILMED
4 -78
DDC

DNA 4253F

LIMITATIONS ON THE SIZE OF EJECTA CRATERS

Applied Theory, Inc.
1010 Westwood Boulevard
Los Angeles, California 90024

November 1975

Final Report for Period 1 April 1975—31 July 1975

CONTRACT No. DNA 001-75-C-0298

APPROVED FOR PUBLIC RELEASE;
DISTRIBUTION UNLIMITED.

THIS WORK SPONSORED BY THE DEFENSE NUCLEAR AGENCY
UNDER RDT&E RMSS CODE B344075464 Y99QAXSA00176 H2590D.

Prepared for
Director
DEFENSE NUCLEAR AGENCY
Washington, D. C. 20305

UNCLASSIFIED

SECURITY CLASSIFICATION OF THIS PAGE (When Data Entered)

REPORT DOCUMENTATION PAGE

READ INSTRUCTIONS BEFORE COMPLETING FORM

1. REPORT NUMBER: DNA 4253F
2. GOVT ACCESSION NO.
3. RECIPIENT'S CATALOG NUMBER

4. TITLE (and Subtitle): LIMITATIONS ON THE SIZE OF EJECTA CRATERS.

5. TYPE OF REPORT & PERIOD COVERED: Final Report 1 Apr [redacted]—31 Jul 75

6. PERFORMING ORG. REPORT NUMBER: ATR-75-44-1

7. AUTHOR(s): John G. Trulio, Neil K. Perl, Raymond W. Latham

8. CONTRACT OR GRANT NUMBER(s): DNA 001-75-C-0298

9. PERFORMING ORGANIZATION NAME AND ADDRESS: Applied Theory, Inc., 1010 Westwood Boulevard, Los Angeles, California 90024

10. PROGRAM ELEMENT, PROJECT, TASK AREA & WORK UNIT NUMBERS: Subtask Y99QAXSA001-76

11. CONTROLLING OFFICE NAME AND ADDRESS: Director, Defense Nuclear Agency, Washington, D.C. 20305

12. REPORT DATE: Nov [redacted] 75

13. NUMBER OF PAGES: ~~84~~ 82 pp.

14. MONITORING AGENCY NAME & ADDRESS (if different from Controlling Office): DNA, SBIE; 4253F; AD-E300 087

15. SECURITY CLASS (of this report): UNCLASSIFIED

15a. DECLASSIFICATION/DOWNGRADING SCHEDULE

16. DISTRIBUTION STATEMENT (of this Report)

Approved for public release; distribution unlimited.

17. DISTRIBUTION STATEMENT (of the abstract entered in Block 20, if different from Report)

18. SUPPLEMENTARY NOTES

This work sponsored by the Defense Nuclear Agency under RDT&E RMSS Code B344075464 Y99QAXSA00176 H2590D.

19. KEY WORDS (Continue on reverse side if necessary and identify by block number)

20. ABSTRACT (Continue on reverse side if necessary and identify by block number)

A simple model has been developed to compute the shapes of ejecta craters, and to set upper bounds on their sizes, using only data from spherically-symmetric fields of motion. The model was constructed in stepwise fashion to account for (1) relief of direct-induced stresses near the ground surface, with ensuing upward ground motion, (2) downward migration of the center of pressure in the ground as shock-vaporized material → next page

DD FORM 1 JAN 73 1473 EDITION OF 1 NOV 65 IS OBSOLETE

UNCLASSIFIED

SECURITY CLASSIFICATION OF THIS PAGE (When Data Entered)

387244

20. ABSTRACT (Continued)

cont → expands upward, (3) downward acceleration of a continuous ground medium by overpressure, and (4) downward acceleration of a fragmented ground medium by overpressure. Step (4) is not yet complete; at its conclusion, the combined effects of overpressure and direct-induced stresses - effects that do not follow the rules of simple scaling - will be included in the model.

Near-surface motion of the ground was computed as a function of range, time and coupled-energy-fraction at the increasing stages of complexity represented by steps (i), (ii), and (iii). The results are presented in graphs for tuff, salt, limestone and granite half-spaces. The principal result obtained so far is that with the coupled-energy fractions presently accepted for nuclear surface bursts in the megaton range, even the coarse upper bound of the present model limits ejecta craters to radii of 990, 1060, 1220 and 1230 ft, respectively, for the four half-space materials. From step (iii) slightly smaller craters are found than from step (ii), and the craters resulting from step (iv) will be smaller still.

Deformation of the ground in which material elements experience inelastic shear strains but remain part of a solid continuum (plastic flow), forms a second major crater-producing mechanism. A loose upper bound was established for the fraction contributed by plastic flow to the total volume of a canonical crater. If 8% of the yield is coupled to the ground - the maximum according to present estimates - we find that craters cannot be produced by plastic flow alone in materials whose von Mises limits of strength exceed .42 ksi; also, plastic flow will not account for more than 10% of the volume of a canonical crater in a material whose von Mises limit of strength exceeds 6.2 ksi. If 4% of the yield is coupled, then the corresponding von Mises limits become .19 ksi and 2.8 ksi.

TABLE OF CONTENTS

TABLE OF CONTENTS (Continued)

SECTION 1

INTRODUCTION

1.1 Ejecta Formation

Advances in computational techniques in the past few years have made it feasible (from a numerical standpoint at least) to calculate the motion of material during the formation of craters from near-surface nuclear explosions, given the mechanical properties of the medium around the crater and the field of motion at the close of the early radiation-hydrodynamic phase of the burst. Yet, when the computational models are applied to the problem of crater formation from a nominal nuclear explosion (1 megaton (MT) yield) at the surface of a reasonably stiff geologic medium (i.e., with a P-wave speed on the order of 10^4 ft/sec), the volume of the resulting numerical crater is characteristically too small[1] by a factor of about fifty. A discrepancy of that magnitude, while discouraging, is nevertheless consistent with results obtained five years ago in the first calculations of ejecta formation in similar bursts; the resulting ejecta masses were "too small by at least a factor of forty",[2] and in several cases by a factor closer to 100. The fact that in more recent calculations crater volumes have also proven too small by about the same factors is almost certainly not a coincidence, as a short review of the relation between crater volume and ejecta mass will show.

Crater formation can take place by any combination of three known mechanisms, namely, compaction, plastic flow away from ground zero, and ejecta production. By "compaction" is meant the irreversible removal of gas-filled spaces distributed more or less uniformly through a matrix of solid material; the spaces can form a continuous

network of channels (but need not), while the solid matrix is simply-connected. Plastic flow is a process whereby irreversible shear strains are imparted to material elements that form a simply-connected continuum. Ejecta production refers to upward acceleration of fragmented ground material into gases above the crater region; fragmentation, to the extent that it results from the burst itself, is considered part of the process of ejecta production.

At present the geologic media of principal military interest are either competent or nearly saturated. In such materials, compaction will not account for a significant fraction of the crater volume, while plastic flow and ejecta production generally both contribute significantly to a crater's ultimate size. However, the fractions of the crater volume that result from plastic flow and ejecta production in a 1 MT surface burst are not known experimentally, and calculations in which predicted crater volumes equal about 2% of the observed volumes would appear an unreliable source of such data. In general, we would expect ejecta production to be responsible for most of the volume of a crater in a highly competent rock (again, for a 1 MT surface burst), while plastic flow probably dominates crater formation in less competent, but nearly-saturated, materials. Furthermore, it is reasonable to expect that when stress levels in the ground are so low that calculated ejecta masses are too small by a factor of 40 to 100, then the crater volume accounted for by plastic flow will also be seriously underestimated.

For the reasons stated, and omitting compaction craters as having little or no military interest at present, we generally expect ejecta masses and crater volumes to be closely related. That expectation is evidently consistent with observations of

at least some explosion and impact craters[3], in which ejecta production has been found to account for at least 80% of the crater volume.

1.2 Direct-Induced Motion, Airblast-Induced Motion, and the Breakdown of Simple Scaling Rules

The work reported here was motivated mainly by the observation that both the mass and velocity of ejecta produced in a near-surface explosion can depend critically on the balance struck between two competing processes. On the one hand, energy released in a near-surface explosion is found in part in gases above the ground surface, and the resulting overpressure acts to drive ground material downward. The remainder of the energy is delivered to the ground where it generates compressive stresses; those stresses, in the absence of significant overpressure, would be relieved at the ground surface, throwing material upward.

Surely, the two processes just noted are real, and one of them tends to suppress ejecta formation while the other enhances it. What one might be included to dispute out of hand is the further assertion that the balance between the two processes can be so critical that an increase of 10 or 20% in directly-coupled energy can result in an order of magnitude increase in ejecta mass. On examining the objections to that idea that have so far come to our attention, we find them joined by one common thread, namely, the intuitive notion that in rough approximation at least, the rules of simple scaling relate the amount of energy coupled to the ground to the mass of ejecta produced in a nuclear burst. On that basis, ejecta mass would be simply proportional to the amount of coupled energy, and the balance struck between overpressure and direct-induced stress would be irrelevant for purposes of ejecta production.

The notion that ejecta production takes place in accord with the rules of simple scaling of the direct-induced field,

appears widespread. It is therefore appropriate to review briefly the rules of simple scaling, their basis and limitations, and some consequences of their breakdown that we believe are particularly relevant to the formation of ejecta craters.

1.2.1 Crater Formation under Conditions of Simple Scaling

Suppose that two fields of motion evolve in such a way that the velocity, stress and specific internal energy found in one field at an arbitrary time t and position $\underline{r}$, are found in the other at the time αt and position $\alpha \underline{r}$, where α is a constant. The two fields are then said to be simply-scaled versions of one another, and α is referred to as the scale-factor that converts one field to the other. Under certain conditions two fields that happen to be simply-scaled versions of one another at one instant of time will remain so thereafter. In particular, two fields related by a scale-factor at one instant will continue to be related by that factor if (a) imposed stresses and/or velocities on the boundaries of the two fields are simply-scaled versions of each other, (b) stress increments are determined only by increments in strain and internal energy, and (c) the forces on particles of matter are determined by material stresses alone.

In a commonly held view of crater formation, the distribution of energy coupled to the ground in the early radiation-hydrodynamic ("rad-hydro") stages of a nuclear surface burst is roughly similar, in the sense of simple scaling, for all bursts, and conditions (b) and (c) apply in reasonable approximation. Under such conditions it follows that if the directly-coupled energy E_c is varied by some small positive amount δE_c, then the field of motion will be unchanged except that the velocity and stress (and all other intensive dynamic and thermodynamic variables) of the original field will be found in the varied

field at positions and times that increase by the factor $(1 + \delta E_c/E_c)^{\frac{1}{3}}$. With $0 < \delta E_c/E \ll 1$, the factor $(1 + \delta E_c/E_c)^{\frac{1}{3}}$ can be simplified to $(1 + \frac{1}{3}\delta E_c/E_c)$.

If the overpressure is neglected, then we conclude that ejecta velocities at a given range, R, and time, t, in the original field are found in the varied field at a range, R*, and time, t*, that are greater than the original values (R,t) by the factor $(1 + \frac{1}{3}\delta E_c/E_c)$. The mass of ejecta rising through the original ground surface plane per unit area and time will be the same at (R,t) as at (R*,t*), but the area associated with that flux is larger in the varied field by the factor $(1 + \frac{2}{3}\delta E_c/E_c)$, while equal changes in flux take place over a time that is longer by the factor $(1 + \frac{1}{3}\delta E_c/E_c)$. Hence, the total ejecta mass is larger in the varied field by the factor $(1 + \delta E_c/E_c)$, i.e., a 2%, 3% or 10% increase in coupled energy leads to a 2%, 3% or 10% increase in ejecta mass - the familiar result of simple scaling.

1.2.2 The Breakdown of Simple Scaling

According to present best estimates, only about 50 kilotons (KT) of energy are found below the original ground surface plane when the radiation-hydrodynamic ("rad-hydro") phase of a 1 MT surface burst ends. After the rad-hydro phase, vaporized earth streams through the original ground surface plane and mixes with the fireball gases above. As a result, considerably less energy than 50 KT ever resides in condensed ground material, over the entire period from burst initiation to the time when crater formation is complete. Thus, while the maximum energy ever found in ground material in all forms is about 80 KT, most of that energy has little influence on ground motion. Evidently, the total coupled energy that contributes to crater formation is not easy to assess with precision, but according

to present coupling calculations that energy cannot be reckoned as greater than about 8% of the device yield at any time - a small fraction. Doubling that fraction will not reduce by more than about 9% the energy that resides in the fireball. As a result the overpressure will not be affected much by what amounts to a large change in directly-coupled energy.

For simplicity, let us assume that changing the fraction of coupled energy (which we equate to the maximum energy residing in ground material during the rad-hydro phase; Section 1.3.2), produces only a simple scale-change in the energy distribution. Such an assumption is reasonable; there is no obvious reason why the shapes of direct-induced isobars, etc., during the rad-hydro phase should be sensitive to the amount of energy coupled. As a result, if stress increments depend only on increments in strain and internal energy, one might be tempted to conclude that the two fields of ground motion will be related by the rules of simple scaling forever after. Not so.

In particular, if the rules of simple scaling are to apply to the ground-motion field, it must either be the case that (a) the overpressure, as a function of range and time, is subject to the same scaling factor as the coupled-energy distribution, or (b) the overpressure has no significant effect on crater or ejecta formation. Proposition (a) is clearly false; the overpressure is only slightly changed by doubling the energy coupled to the ground. Proposition (b) could be true, and in fact we believe it to be a good approximation for many burst conditions of real interest. However, to consider proposition (b) correct in general, or for a 1-MT surface burst in particular, must be recognized for what it is - an unsupported hypothesis.

We now ask what qualitative effects overpressure has on ejecta in the original and varied fields of Section 1.1.1. We can of course observe that overpressure tends to suppress ejecta formation in both fields. However, to arrive at a meatier qualitative conclusion, we note that on the crater region, the airblast wave far outruns the direct-induced pulse; we also recall that (as canonically represented) overpressure is nearly independent of range and decays continually with time as the direct pulse sweeps over the crater region.[4] The overpressure is therefore greater at the range R and time t than at the range $R(1+\frac{1}{3}\delta E_c/E_c)$ ($\equiv R^*$) and time $t(1+\frac{1}{3}\delta E_c/E_c)$ ($\equiv t^*$). Hence, overpressure impedes the creation of ejecta less in the varied field (with its larger fraction of coupled energy) than in the original field. As a result, when overpressure effects are included, an increase in coupled energy results in a greater increase in ejecta mass than would be predicted by simple scaling.

The quantitative effects of overpressure on the formation of ejecta evidently depend on the evolving overpressure and direct-induced fields. To explore that relation is a prime motive of the program described here.

1.2.3 Pressure Equilibration Around Nascent Ejecta Fragments

According to state-of-the-art descriptions of nuclear surface bursts in the megaton range, the downward-directed impulse delivered to the ground by the pressure of fireball gases ("overpressure") depends only on device yield. Neither variations in the properties of the ground, nor in the small fraction of the yield coupled to the ground, affect the canonical overpressure. Actually, air-ground interactions have had substantial effects on overpressure in calculations of the full field of flow, particularly in the region of the crater, but those interactions are very complex and depend strongly on the

distribution of ejecta-fragment sizes.[5,6] Thus, while corrections to the canonical overpressure could make large changes in the size of calculated ejecta-craters, no reliable procedure is known for including the effects of gas-ground interactions in the description of overpressure. However, our main purpose at the moment is to call attention to another point, to wit: The downward velocity increment delivered by fireball gases to near-surface ground material is much different for a continuous earth medium than for a disintegrating and fragmented ground medium. That fact must be faced whether the canonical overpressure is correct or not, as will now be explained.

The impulse delivered by overpressure per unit mass of disturbed ground - which is equal to the average downward increment in ground velocity produced by that impulse - is evidently inversely proportional to the mass of ground through which the overpressure pulse travels. That mass is maximized, and the velocity increment minimized, if the ground holds together as a continuum. In that case the pulse travels with at least the speed of sound in the ground medium. On the other hand, if the overpressure pulse, in its downward journey, arrives at a free surface created by fragmentation of ground material, then it propagates no deeper until a gap between opposed free surfaces closes. However, the rate of closure of a gap between two solid masses is determined by the speed with which those masses move, and is generally much smaller than the speed of sound in the solid. Thus downward overpressure-impulse can become trapped in a relatively small mass of earth, in which case a large downward increment in velocity will be imparted by that impulse to near-surface ground material.

To illustrate the point, and thereby obtain a clearer picture of the pertinent physical processes, suppose that

a cube of earth one foot on an edge begins to separate from the main mass of upthrust earth at a velocity of 100 ft/sec. It will then take at least 10 ms for that block to fly clear of surrounding fragments. During that 10-ms period, if we suppose the fragment lies at a range of 750 ft from ground zero, an overpressure of perhaps 50 bars will act on the upper surface of the block, while the stress below could remain at a value very nearly equal to zero. A downward velocity of over 200 ft/sec would then be imparted to the block by overpressure, and the block would simply not be ejected. However, fireball gases would flow into cracks around the block and might, by equalizing pressure all around its surface, cut short the period of downward acceleration. With such considerations in mind, the process of gas diffusion into cracks around nascent ejecta fragments has been studied in some detail, and a basis has been set down for detailed calculations of gas-ground interaction during the break-away phase of ejecta formation.[7] While such calculations have yet to be performed, it is nevertheless clear that the degree to which overpressure opposes ejecta formation is greatly underestimated by treating the ground as continuous; overpressure-impulse is then spread over an unrealistically large mass of ground material, and the downward velocity imparted to near-surface material is proportionately too small.

1.2.4 Downward Migration of the Center of a Near-Surface Nuclear Explosion

Another important process (but less important in surface bursts than details of nascent ejecta formation) is encountered early in the history of a near-surface nuclear explosion, when ground vaporizes. Specifically, the center of approximate spherical symmetry of the direct-induced field moves downward into the ground to a significant depth.[8] After vaporization (due to high shock pressure early in the motion) ceases, the center of symmetry remains

nearly fixed in depth. The significance of such source migration lies in the fact that material at shallower depths than the source receives an upward vertical component of velocity as the direct-induced pulse passes over it; that contribution to the vertical velocity of near-surface material could (depending on the depth reached by the center of the burst) be larger than the contribution due to relief of compressive vertical stress at the ground surface.

It is appropriate here to explore more fully the process of center-of-burst migration. To that end, we consider a ground medium at whose surface is found a hemispherical region about 5 ft in radius, in which about 50 kilotons (KT) of energy are uniformly distributed. In that way, albeit crudely, we approximate the distribution of energy in ground material at the close of the rad-hydro phase of a nuclear surface burst. In actual calculations of rad-hydro coupling, the distribution of energy is not uniform, some ground material has already blown upward into the fireball region, and some energy resides in a thin sheet of surface material out to a range perhaps ten times that of the hemisphere considered here. However, those details of the distribution of coupled energy are not essential to an account of source migration, and their inclusion here would only impede understanding of the migration process.

Energy densities on the order of 10^{15} erg/gm would be found on the idealized deposition region contemplated; all materials exist as hot vapor at such energy densities. Also, since the multi-megabar pressures exerted by such ground material greatly exceed the pressures found in gases above the ground, vaporized ground material will expand rapidly upward. At the same time, a multi-megabar shock will be driven downward into previously undisturbed ground below. Ground material subjected to that shock will

vaporize, and will also acquire a downward velocity on the order of 10^5 ft/sec. Since the speed with which vaporized ground expands upward into the fireball is even greater than 10^5 ft/sec, a very strong rarefaction follows the shock. As a result, the stagnation point of the flow, where material has zero vertical velocity, trails the shock closely. A similar process takes place in non-vertical directions of propagation of the shock front, up to the horizontal ground-surface plane. However, the shock pressure decays at a rate that changes rapidly with the direction of shock propagation. Not only are the more nearly horizontal directions of propagation closest to the ground surface, where the rarefaction due to upward expansion of vaporized ground is felt soonest and most strongly, but divergence of the shock moving radially outward from the symmetry axis further erodes the pressure driving the shock. Thus on any part of the shock front whose normal has an appreciable horizontal component, the pressure drops relatively soon to levels at which shock heating is not sufficient to vaporize ground material; at the same time, vaporization continues down the axis of symmetry. As a result, a rather long and narrow cylindrical hole is dug where vaporized ground expands upward into the fireball. In fact, well before vaporization ceases altogether, the discharge of vaporized ground into the fireball comes to resemble the supersonic flow of gas out of a cylindrical pipe. In this case, however, the gas is generated only as a result of shock-heating of ground material, and less and less heat is developed as the trailing rarefaction erodes the shock pressure.

At the time vaporization of ground material stops altogether, the stagnation point of the flow along the symmetry axis is nearly coincident with the shock front itself. As already noted, near-coincidence of those two axial points is a consequence of the severe rarefaction that attends upward expansion of vaporized ground -

an expansion that results in much lower pressures than those of just-shocked material. Evidently, the highest pressures in the field are found near the stagnation point at the time when vaporization ceases; stresses in and around the hole above the stagnation point are far lower than those at the bottom of the hole, where the shock front is located. Thus, hot high-pressure material in a hemispherical region at the ground surface gives rise to a deeper-lying localized region of heated solid at high pressure - but at temperatures and pressures not nearly so high as in the initial hemisphere; in short, the apparent center of the explosion - its "epicenter" - has migrated downward into the ground.

After vaporization ceases, no further significant migration will take place because the rarefaction that trails the shock front in condensed material adds only a small positive increment to the material's vertical velocity. In that respect the behavior of just-shocked material changes drastically when vaporization stops. To explain that sudden change, we note that in condensed material very little expansion is required to cause a large drop in pressure, and the velocities produced as shock-liquefied ground expands are therefore much smaller than those of freely-expanding vapor. Thus, the stagnation point on the symmetry axis remains almost stationary after vaporization stops, and a compression wave runs outward, more or less radially, in all directions from that point.

1.3 Outline of the Program

Since the calculated dimensions of craters produced by nuclear surface bursts are far smaller than experimental data would suggest, our primary aim in the present program has been to establish maximum contributions to crater size from the physical processes discussed in Section 1.2. To that end, we have devised procedures for utilizing spherically symmetric fields

of motion to obtain the upper bounds sought. Those procedures and their rationale are described qualitatively below; quantitative results obtained for each of the processes of Section 1.2, and details of the derivation of those results, are presented in Section 2. The factors that led us to restrict attention to cratering in homogeneous half-spaces, and to choose the ranges of other system parameters covered in the study, are discussed in this section.

1.3.1 Craters in Homogeneous Half-Spaces

No nuclear surface bursts in the megaton range have taken place at sites like those addressed in past cratering calculations. Hence, there are no absolute contradictions between observed crater dimensions and those calculated. However, while it is conceivable that the craters calculated for such sites as U-2 are approximately correct in size, that possibility appears extremely remote. Neither have we found any convincing reason to suppose that present computational difficulties in describing crater formation will be resolved by more accurate models of the lithosphere. On the contrary, for the earth media of interest here (comprised of nearly saturated and/or competent materials), layering produces no striking changes in ejecta fields, relative to the fields calculated for megaton surface bursts on homogeneous half-spaces. Moreover, at many real sites (e.g., large granite or salt masses) the lithosphere appears reasonably well represented as a homogeneous half-space, at least on the scale of crater dimensions. Hence, considering the magnitude of the apparent discrepancies between calculated and observed crater dimensions for nuclear surface bursts, no useful purpose would be served at this time by considering more complicated geologic media than homogeneous half-spaces. Accordingly, only homogeneous

half-spaces have been addressed in this study.

The choice of half-space materials was determined largely by the availability of calculated fields of motion for tamped nuclear bursts; as explained below (Section 1.3.3), fields of that kind comprise the data base for the cratering model developed and applied in this program. Fortunately, the rules of simple scaling (Section 1.2.1) hold with negligible error for tamped fields, so that knowledge of the motion produced by a tamped burst for a single nuclear yield suffices to determine the motion for any other yield. In all, the cratering model was exercised for four different half-space materials, namely, tuff,[9] salt,[10] granite,[11] and limestone.[11] The variety of mechanical properties presented by those materials suffices to characterize a considerable portion of the total range of surface-burst environments commonly encountered.

In considering possible descriptions of mechanical properties themselves, we were influenced by the fact that calculated masses of ejecta have so far proven material-dependent to the extent of about a factor of 10. Also, the sources of present difficulty in calculating cratering motion could lie in inadequate representations of material properties. Hence, the full apparatus of current constitutive models has been retained in the present study.

1.3.2 Coupled Energy

In describing migration of the epicenter of a nuclear surface burst (Section 1.2.3), we found it convenient to refer to "coupled energy." Yet, to talk of "coupled energy," and of a fraction of the device coupled to the ground, is to speak rather loosely. It is true that at any given time after detonation a definite fraction of the yield will reside in earth materials,

wherever they may be at that time and in whatever state. However, given the objective of crater-size prediction, it is unrealistic to disregard the location and state of energized material. For example, ejecta fragments that travel far from the crater and then become vaporized by conduction of heat from fireball gases, will thereby have acquired part of the explosive yield. However, the same amount of energy deposited a few feet below ground zero at bang time would have a much larger effect on the crater. Again, one might observe that most of the energy delivered to ground material "ends up" as heat, but there's more to the story. In the "end," the heat (mainly shock-generated) will radiate away[12] and the portion of the yield "permanently" coupled to ground material will be found mainly in the form of chemical energy. To define "coupled energy" as only that portion of the yield deposited in the ground in chemical form would be to ignore the role played in crater formation by kinetic energy that later becomes converted to heat in solid earth--a poor choice. Thus, even if we define the energy coupled to the ground as the burst-induced change in energy of all ground material, wherever it may be and whatever its state, we arrive at no single value of a coupled energy fraction. Rather, the coupled energy so defined varies greatly with time. Yet, despite its fuzziness, the idea of dividing the yield into coupled and noncoupled fractions is useful, and we subscribe to the concept. At the same time, the arbitrariness implicit in the definition of a "coupled energy fraction" should be recognized; assigning to that fraction a numerical value that will correlate well with crater size, presents a problem with no unique solution.

We (and others[13]) suggest that the maximum energy delivered to the ground during the rad-hydro stage of a burst be regarded

as the energy coupled to the ground. That maximum is generally reached during interaction of bomb debris with the ground, and amounts to about 8% of the yield for surface bursts in the megaton range (at least according to the coupling calculations currently in favor). The energy residing in ground material when rad-hydro motion ends (a not-too-well-defined time) comprises about 4% of the yield.

The suggested definition of coupled energy does not entail a division of the ground into a portion whose energy contributes to cratering, and a portion that does not. Yet, by selecting as the "coupled energy" the change in energy of all ground material up to the time suggested, the problem of unreasonable spatial distribution of coupled energy is circumvented; the time chosen occurs so soon after burst initiation that all disturbed ground material lies below, or very close to, the original ground-surface plane at that time. Moreover, since we aim to place an upper bound on the effects of various physical processes on crater size, the maximum energy delivered to the ground during the period of rad-hydro motion is more useful in computing approximate fields of motion near the burst point than is the energy at the end of that period.

Ultimately, the value of a definition of coupled energy will lie in its degree of correlation with a single cratering parameter, such as volume. To decide among the more likely definitions on the basis of present nuclear cratering experience, however, is not possible, because that experience is severely limited. Furthermore, empirical correlation with a parameter like crater volume could lead to an optimum "coupled-energy" quantity with no apparent relation to any actual coupled energy. Hence, in view of its present uncertainty, the fraction of the yield coupled

to the ground has been treated in the work reported here, as a variable, to which we have assigned values from 3% to 10%.

1.3.3 Spherically Symmetric Fields and Maximum Crater Dimensions

None of the energy coupled to the ground in tamped explosions leaves the ground. By contrast, all but a small fraction of the maximum energy coupled to the ground during the rad-hydro phase of motion escapes to the fireball before any significant cratering action occurs[14]. As a result, tamped spherical bursts can be used to provide the basic data for (a) upper-bound estimates of crater dimensions, and (b) determining the sensitivity of those bounds to the processes of Section 1.2.

Energy coupled to the ground during rad-hydro motion is distributed over a roughly hemispherical region of earth. Accordingly, to bound the motion produced by a surface burst in which a fraction α of the total yield W is delivered to the ground, our plan has been to use in an appropriate way the field of motion produced by a tamped burst of yield $2\alpha W$. Thus, at the core of the cratering model described here is a picture of a nuclear surface burst in which a fraction of the yield enters the ground at a very early stage of the explosion, and is prevented from escaping thereafter by a ground surface that we consider absolutely rigid and perfectly reflecting. Since no energy leaves the ground, both the peak radial stress and velocity at any range should greatly exceed those found on the crater region in a surface burst (except on the original small region of energy deposition). Of relatively minor physical consequence, but very convenient for purposes of calculation, is the further assumption that the coupled energy is distributed in spherically-symmetric fashion.

To turn exaggerated stress and velocity amplitudes associated with a rigid perfectly-reflecting ground surface, into exaggerated estimates of the effects of the processes discussed in Section 1.2., is a fairly simple matter, and is discussed below. Let us first observe, however, that a spherical approximation to a direct-induced field, even when coupled with a uniaxial version of airblast-induced motion, will not reproduce physical phenomena that depend intrinsically on two independent spatial coordinates. For our purposes, Rayleigh waves appear to present the most important example of that kind of phenomenon, since they offer a mechanism for concentrating energy near the ground surface that our model does not take into account. A cursory study of Rayleigh-wave motion has therefore been conducted to help determine whether the present model provides upper-bound near-surface motions. Results of that study are also presented below.

1.3.4 Upward Ground-Surface Motion Without Overpressure

Let σ_M denote the peak radial stress produced at a given range R from a spherical burst of yield $2\alpha W$. Then, at a distance R from a small region at the ground surface containing the coupled energy αW, the peak horizontal stress would also equal σ_M if the ground-surface plane were rigid. At the time when the peak radial stress σ_M is attained at range R for the spherical burst, so is the peak azimuthal stress - and hence also the peak vertical stress along a rigid ground-surface plane at range R from coupled energy αW. The peak values of vertical stress so delivered lead directly to an upper bound U_{max} on the peak vertical velocity that develops in near-surface material, when direct-induced stresses at any given range are relieved, in the complete absence of overpressure, by upward motion of the ground.

To produce the bound U_{max}, the peak vertical stress at each range is divided by the loading-wave impedance of near-surface material. In so computing U_{max}, we implement a simple picture of upward jump-off of ground-surface material not confined from above, upon being disturbed by a horizontally-traveling pulse. The pulse is driven by an energy source that experiences none of the depletion associated in a surface burst with the discharge of vaporized ground into the fireball, and is also not affected by the release wave produced when nearby ground material jumps upward. Hence, the peak stress carried by the pulse should be considerably higher at any given range than would actually be the case in a surface burst. The peak vertical velocity U_{max} should therefore also be higher.

1.3.5 Downward Migration of the Center of the Burst

The second effect incorporated into our model of near-surface ground motion is downward migration of the center of the burst, or "burst epicenter" (Section 1.2.4). The effect on near-surface motion of the epicenter's having come to rest below the ground surface plane is to add an increment of vertical velocity to the peak vertical velocity resulting from stress relief (just discussed; Section 1.3.4). To compute the additional increment in vertical particle velocity, we again look to the spherical field produced by a tamped burst of yield $2\alpha W$. In particular, the vertical velocity increment is taken as the product of two factors, namely, (i) the peak radial particle velocity behind the pulse arriving at a given range in the tamped spherical field, and (ii) the sine of the angle $\theta(R)$ made with the horizontal by the line joining the epicenter to the ground-surface point at range R.

To determine the angle $\theta(R)$ requires knowledge of the depth of the epicenter, a quantity that could be evaluated by referring to past calculations of nuclear surface bursts. Instead, we have

chosen to make consistent use of spherical tamped bursts as a means of overestimating the effects of various physical processes on crater formation. In the present instance, the greatest range at which material vaporizes in the tamped field is taken as the final depth reached by the center of the burst. Once again, the absence of energy transfer from vaporized ground to the fireball tends to produce an overestimate of the physical quantity sought. In particular we expect retention of energy in the ground during a tamped burst to result in overly-strong backing of the direct shock driven by the burst, and hence in shock vaporization to a greater distance from the burst-point than would be found in an actual surface explosion. On the other hand, the streamlines followed by vapor generated at the shock front in a surface burst diverge less strongly than those of a spherical field, compensating to some extent for loss of energy to the fireball. On balance, we find that the two effects very nearly cancel, so that the maximum range of shock vaporization in a tamped spherical burst is about equal to our best present estimates of the depth reached by the epicenter in a surface burst. Thus, as far as we know, the upward component of particle velocity behind the direct-induced pulse at the ground surface at any given range is neither significantly exaggerated nor understated here.

1.3.6 Downward Velocity Imparted by Overpressure to a Continuous Earth Medium

As canonically represented,[4] the overpressure from a nuclear surface burst is smallest at ground zero, greatest at the front of the airblast wave, and varies overall by a factor of 2.6. However, the variation in overpressure with range amounts to 10% or less between ground zero and a point 5/6 of the distance to the front of the airblast wave. Also, even with 10% of the yield coupled to a granite half-space, the direct pulse propagates to

less than 800 ft of range at a time when the airblast wave reaches 1200 ft, for a yield of 1 megaton. Hence, to set a somewhat more realistic limit than zero on the minimum ejecta-supressing effect of overpressure, we consider the vertical impulse delivered by overpressure to become distributed over ground material by means of a uniaxial loading wave that propagates downward into undisturbed ground. Vertical motion is then driven by an airblast wave that varies with yield, range and time, but that follows the rules of simple scaling with respect to yield. As a result, knowledge of the vertical motion induced in a half-space by the airblast load at a single range from a burst of given yield, implies similar knowledge for any other yield.

Fortunately, for the four materials studied here fields of vertical unaxial motion have been calculated in the past under airblast loading appropriate to a number of simply-scaled ranges; some further calculations of the same kind were performed as part of the work reported here. As a result, tables are available from which the downward velocity increment due to overpressure can be obtained at each of several ranges, at any given time of arrival of the direct wave generated by energy coupling.

The direct-induced fields to which the spherical calculations provide overestimates of stress, expand at a considerably slower rate than the fireball. Thus, the outgoing direct-induced pulse travels through near-surface material already subjected to loading, and to partial unloading, in response to overpressure. Some air-void space is therefore removed from the material before its disturbance by the direct-induced signal. Neglect of that process would have almost no consequences for granite and limestone, since those two materials have difficult-to-remove, and very small, air-void-fractions. For salt, however, pre-compaction due to airblast loading could reduce significantly

the rate of attenuation of the direct wave near the ground surface, while in the tuff the rate of attenuation would most likely undergo a substantial reduction. The resulting enhancement of the upward vertical velocity imparted to near-surface material by the direct wave would be partly offset by the material's increased impedance, and in any case does not appear to outweigh the downward velocity increment due to overpressure.

The fact that the medium is set in downward motion by overpressure is of no consequence to the development of the direct-induced field; the two motions couple only to the extent that the initial stress-strain state changes during passage of the overpressure-induced pulse - and except for tuff, the effects of those changes are small-to-negligible. Hence, the changes in velocity produced by direct-induced motion can, with little error, be added to the velocity induced by overpressure; for linear elastic media (to which limestone and granite consitute close approximations at the stress-levels of consequence here); the two motions are entirely separable. Thus, we simply add the direct- and airblast-induced vertical components of velocity to produce another overestimate of peak vertical particle velocity, but not so great an overestimate as was obtained by considering direct-induced motion alone (Section 1.3.5).

1.3.7 Downward Velocity Imparted by Overpressure to a Cracked or Fragmented Earth Medium

In calculations of ground motion from surface and near-surface nuclear bursts, the ground does not remain continuous in the crater region, but cracks extensively - as indeed it must if substantial masses of ejecta are to be produced. In fact, under the applicable condition of near-zero overburden, even spherically symmetric fields induced by tamped explosions develop extensive regions of cracking. Clearly, such crack formation would be enhanced if the rarefaction resulting from upward

motion of the ground surface were superposed on the spherical field. However, the resulting account of the development of regions of cracked material, and of associated ejecta production, would constitute no more than a coarse approximation to the actual process. A simpler procedure than superposition of uniaxial and spherical fields, and probably as realistic, is to suppose that all ejecta fragments are formed during initial upward motion induced by the direct pulse. We opt for the simpler procedure.

As a result of the fragmentation of near-surface ground meterial, overpressure-impulse delivered at a given range after arrival of the direct pulse will be concentrated in a layer of earth much shallower than the depth attained by the front of the overpressure-induced pulse (Section 1.2.5). The time of equilibration of pressure around ejecta fragments can be limited in several possible ways, of which two appear particularly interesting. On the one hand, pressure equilibration could take place during the time in which a typical fragment moves a distance equal to its own length; on the other hand, equilibration could occur by viscous flow of fireball gases through the cracks opening between fragments. Since the latter is potentially the more rapid of the two processes, it is especially useful to permit the spaces between fragments to widen at a rate equal to the peak radial particle velocity found in tamped bursts (Section 1.3.3); that velocity would appear to define the maximum rate of fragment separation that random motion of the fragments would produce.

The time of equilibration should be calculated for each of the two mechanisms noted. In both cases the distribution of ejecta sizes generally accepted as applicable to craters of all kinds,[6] would set the scale of particle dimensions essential to calculations of equilibration time.

1.3.8 Plastic Flow; Depth of the Crater

In a tamped nuclear explosion, shock-induced vaporization of ground material stops before any significant cavity growth has taken place. After vaporization ceases, the same particles are found at all times at the "cavity wall," i.e., the interface between cavity gases and surrounding condensed material. Those particles move rapidly outward at first, but eventually form the wall of a stationary cavity. From past calculations of tamped explosions it is clear that the size of the cavity resulting from such an explosion is determined almost entirely by the von Mises limit of material strength.[5] To explain in detail why the von Mises limit dominates the inelastic deformation processes whereby permanent cavities form is not our present purpose, although it is worth noting that (a) shear stresses in the wall material exceed the von Mises limit by orders of magnitude until the cavity has grown to a significant fraction of its eventual size, and (b) the cavity wall has by then acquired a large outward velocity. The key point here is that the entire cavity volume is accounted for by inelastic deformation of the surrounding medium; moreover, even for the most highly compactible material considered (tuff), plastic flow is by far the most important inelastic process contributing to cavity formation.

The idea of using the cavity from a tamped burst to set a limit on the volume contributed by plastic flow to a surface-burst crater, is suggested by two facts, namely, (i) cavities are created in tamped bursts almost entirely as a result of plastic flow, and (ii) all the energy released in a tamped burst remains in the ground, whereas most of the energy $\propto W$ coupled in a surface burst is soon lost to the fireball. In view of observations (i) and (ii), we take half the cavity volume V_c

resulting from a tamped burst of yield $2\alpha W$ as an upper bound on the portion of the crater volume due to plastic flow. Whether the final cavity radius constitutes an upper bound on crater depth is problematical, but a useful estimate at least is obtained in that way for the depth of a crater.

Although we consider $\frac{1}{2}V_c$ an upper limit on the portion of the crater volume due to plastic flow, we nevertheless recognize that the constraint of spherical symmetry precludes some phenomena that occur during surface bursts. Ejecta formation is perhaps the most obvious and important of those phenomena. Fortunately, the part of the crater volume due to ejecta production and the portion due to plastic flow, can be distinguished from one another with little or no ambiguity, and the distinction is drawn in this study. Another phenomenon not admitted by spherically symmetric fields is plastic flow away from the burst point and tangential to the floor of the crater. The crater would clearly be enlarged by motion of that kind if material slid over the crater lip in the process. However, the overpressure, which must be matched by the normal stress in material at the floor of a crater, provides no impetus to such motion, and even opposes it slightly. More importantly, enlargement of the crater by flow over the crater lip would occur at a rate controlled by the speed with which material moves at the crater bottom, and would therefore require at least a few seconds of time to occur in a 1-MT surface burst. However, over the entire crater region, stress levels appear to fall to within a few bars of their final static equilibrium values well before 1 second has elapsed. In particular, some of our calculations of tamped bursts in salt have been carried far enough to show that even when no energy is allowed to leave the ground in a 1 MT surface burst, and assuming a coupled-energy-fraction of .08 (160KT tamped), no plastic flow takes place out to a range of 1000 ft after .2 sec. In those calculations, the root-mean-squared deviation of the stress

from its final static distribution is smaller than 4800 psi on the crater region .1 sec after detonation, 2500 psi after .2 sec, 380 psi after .4 sec, and 110 psi after .7 sec. At the same times, respective values of overpressure on the crater region are 345, 155, 70 and 37 psi. Thus, it is not difficult to understand why anyone who insists on accounting for crater formation as a process of horizontal plastic flow, must find reasons for believing that geologic solids commonly fail in shear at deviatoric stresses of 100 psi or less.

The same conclusion can be reached more directly by observing that tangential flow is opposed by dissipative shear stresses that continually convert the kinetic energy of flowing material to heat. In particular, suppose that a given medium can deform inelastically, without limit, under a constant shear stress τ. Production of an inelastic shear strain β will then require that heat be generated in amount $\beta\tau$, per unit volume of strained material. Kinetic energy will therefore be lost in at least the amount $\beta\tau$ as a result of the deformation. The reservoir of kinetic energy is limited, however. Specifically, calculations of tamped bursts in granite, limestone, salt and tuff, show that with 8% of the yield coupled to the ground in a surface detonation, the peak radial particle velocity falls to 100 ft/sec at ranges from 550 ft(tuff) to 930 ft(granite), even if the ground surface plane is held at zero altitude after energy deposition takes place. Hence, the product $\beta\tau$ cannot exceed about 150 psi over the outermost quarter of the range-interval covered by a standard crater, if plastic flow is to take place on that interval.

To play a substantial role in enlarging the crater, plastic flow will have to account for horizontal displacements of at least 100 ft; in fact, even a change of radius from 800 ft to 1000 ft, with a proportional increase in depth, would increase the crater volume by only a factor of 2. Accordingly, to arrive at an ap-

propriate value of β, we ask over that depth a horizontal displacement of a few hundred feet at the crater floor would be distributed as shear strain; the smaller that depth, the greater the average shear strain β will be. Since strengths of geologic materials generally increase rapidly with depth, our answer is that the thickness of a plastic flow layer would probably not exceed a few hundred feet, and that the value of the inelastic shear strain β is therefore not likely to be smaller than 1. On that basis, plastic flow will contribute appreciably to crater volume only in materials that fail under smaller shear-stress loads than 150 psi. Even that low value is quite probably an overestimate, since (a) to obtain an upper bound on τ, we have as usual neglected all energy flow out of the ground and into the fireball, (b) over the period of time required for plastic flow, particle velocities in the crater region are smaller by a considerable factor than peak particle velocities, even in the too-strongly-driven spherical fields that follow from assumption (a), and (c) kinetic energy would be consumed by other processes than horizontal inelastic shear (e.g., inelastic hoop strain and work against gravity).

To explore further the limitations imposed on shear strength by conversion of kinetic energy to heat during horizontal plastic flow, we note that only about 1/30 of the energy of a 160-KT tamped burst in granite remains in kinetic form .2 sec after detonation. Suppose then that 1/30 of the maximum energy coupled in a 1-MT nuclear surface burst (80 KT) resides in kinetic form in a vertical cylindrical shell of earth of thickness x, extending downward from the ground surface to a depth d. Let all material in the shell experience an inelastic strain β in horizontal shear against the stress τ, with the result that the horizontal displacement of shell material at the ground surface is x. Then, since β is equal to x/d, and the volume of the shell is proportional to d, the energy dissipated into heat during plastic flow of shell ma-

terial is independent of d. Furthermore, with the shell's inner radius at 750 ft, all its kinetic energy would be converted to heat during 100, 200, 300 and 400 ft of horizontal ground-surface displacement, given respective values of τ of 1137, 267, 112 and 60 psi. Those τ-values are proportional to the entire kinetic energy at a very early time relative to that required for significant horizontal plastic flow, in a field that retains forever the maximum energy coupled in a nuclear surface burst - surely a gross overestimate of the kinetic energy residing in the shells considered.

A second plastic-flow phenomenon excluded from spherical fields is an increase in the depth of a crater near its axis, with equivalent upthrust of material at larger ranges, in a manner similar to the flow of material around a punch pressed into a metal block. Again, however, a second or so after burst initiation, our upper-bound stress levels are so low on the outer portions of a canonical crater that most of the upthrust would probably occur in the crater region itself. Thus, the possibility that two-dimensional plastic flow processes could increase the crater volume to a degree that might compensate for the retention of all coupled energy in cavity formation, seems remote. On the contrary, based on present knowledge of the strengths of geologic materials, it appears that (a) plastic flow contributes to the expansion of the crater mainly while the ground moves outward and downward from the burst point, a process similar to cavity growth in a tamped burst, and (b) the contribution of plastic flow to the crater volume is smaller than $\frac{1}{2}V_c$ by a considerable factor.

It is not clear whether the radius R_c of the cavity produced by the tamped explosive release of energy $2\alpha W$ will bound the depth of the crater formed when energy αW is coupled to the ground in a surface burst. Both the ejection of material from the crater and horizontal plastic flow, as well as combinations thereof, could deepen the crater (and probably do) without altering its volume.

Simply stated, flow divergence is particularly sensitive to radial motion near the symmetry axis where, as a result, outward displacement of material through only a small fraction of the crater volume can add greatly to the crater depth. Hence we consider the radius R_c only as an approximation to the crater depth, and not as bound, even though (a) all coupled energy remains in the ground in a tamped burst, and (b) the overburden opposing cavity growth in the tamped burst is set at only 1 bar.

1.3.9 Surface Waves

Based as it is on calculations of uniaxial and spherical motion, the model of cratering explored here excludes such purely two-dimensional effects as Rayleigh-wave propagation across the crater region. For that reason, two preliminary calculations were made of the motion of a half-space filled with linear elastic material similar to salt. The source for both calculations was defined as the velocity field computed earlier for a tamped burst in salt, at a time when the main outgoing pulse had reached a range (simply-scaled to correspond to a yield of 160 KT) of about 1050 ft. In one calculation the peak particle velocity was obtained at the ground surface as a function of range by solving the full equations of axisymmetric motion. In the other, the field of spherically symmetric motion appropriate to a rigid non-relecting ground surface was computed, and the azimuthal stress from that field was used as described above (Section 1.3.4) to find an upward velocity imparted to near-surface material in the process of stress relief. The resulting particle velocity was then compared with the Rayleigh-wave-dominated velocity computed at the free surface of an elastic half-space, in order to determine the extent to which peak particle velocities might be underestimated in the simple cratering model employed here.

Not surprisingly, the channeling of energy into surface waves leads to a decrease in the rate of decay of peak particle

velocity with range. Thus, on the outer portions of the crater region, still higher bounds on peak particle velocity might have been obtained by including surface-wave effects in our model. However, inelastic deformation, an important process on the crater region, would have interfered so seriously with surface-wave formation that the results noted are inconclusive. Hence we continue to regard the peak particle velocities obtained here as loose upper-bound velocities.

1.4 Principal Results

The main effects of overpressure appear when near-surface material begins to disintegrate into ejecta fragments, and those effects have yet to be incorporated into our estimated upper bound on the vertical velocities of such fragments. A few other subjects requiring further study are noted in Section 3. Nevertheless, several significant results have already been obtained, of which the most important appear in Figures 1, 2, 3 and 4. Figure 1 contains four curves of peak particle velocity vs. range at the surfaces of half-spaces composed of granite, limestone, salt and tuff, respectively. Underlying the curves of Figure 1 is the assumption that 8% of the energy released in a nuclear surface burst becomes coupled to each medium represented in the figure. In addition, it is assumed that all coupled energy remains in the ground - the basic idea used in the work reported here to bound the vertical velocity of material at the ground surface. The curves of Figure 1 also include the effects of downward migration of the burst epicenter (Section 1.3.3), as well as the downward velocity produced by overpressure in near-surface ground material up to the time of arrival of the direct pulse. Figures 2, 3 and 4 contain exactly the same information as Figure 1, but with 3%, 5% and 10% of the device yield, respectively, coupled to the ground.

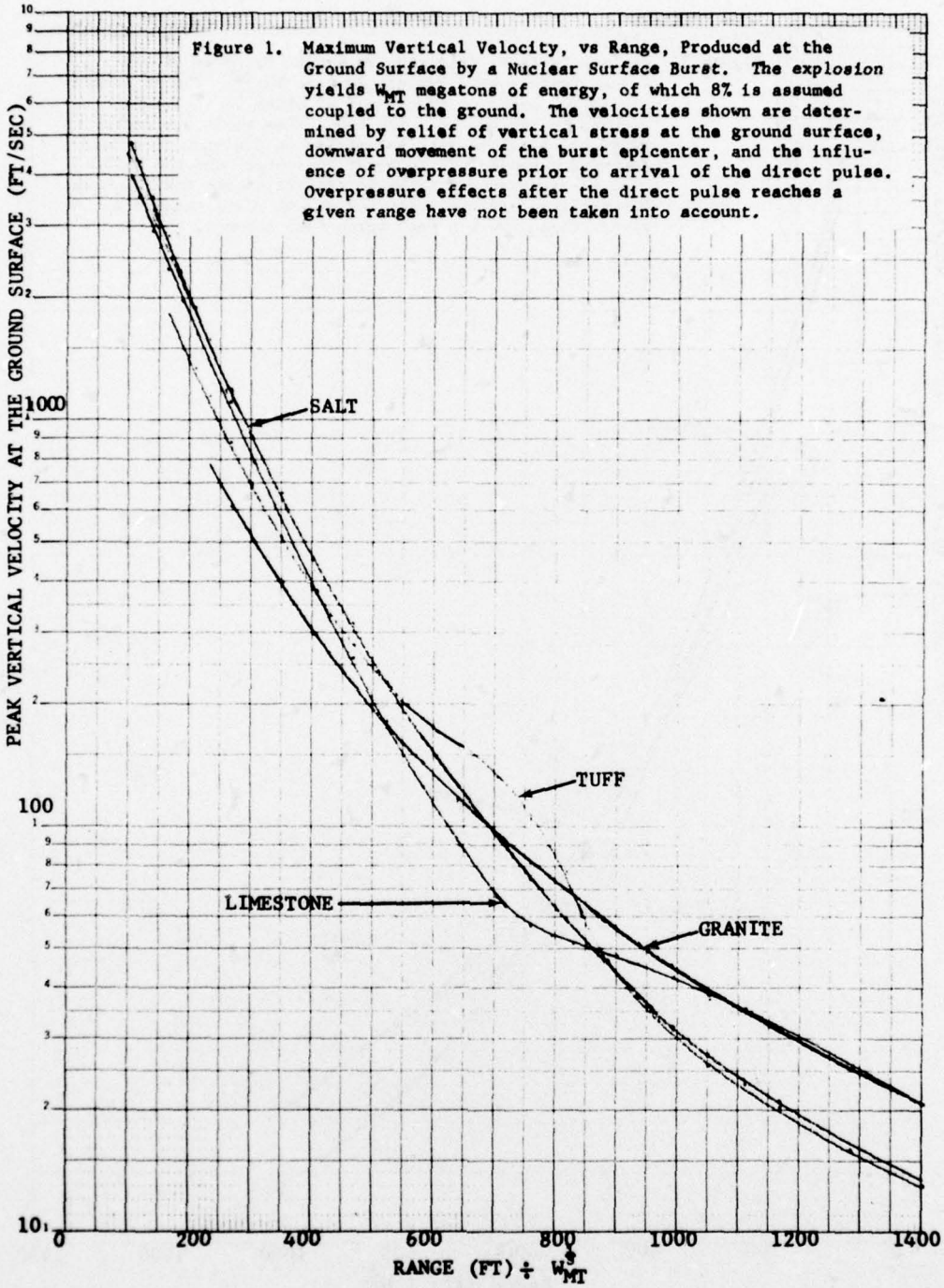

Figure 1. Maximum Vertical Velocity, vs Range, Produced at the Ground Surface by a Nuclear Surface Burst. The explosion yields W_{MT} megatons of energy, of which 8% is assumed coupled to the ground. The velocities shown are determined by relief of vertical stress at the ground surface, downward movement of the burst epicenter, and the influence of overpressure prior to arrival of the direct pulse. Overpressure effects after the direct pulse reaches a given range have not been taken into account.

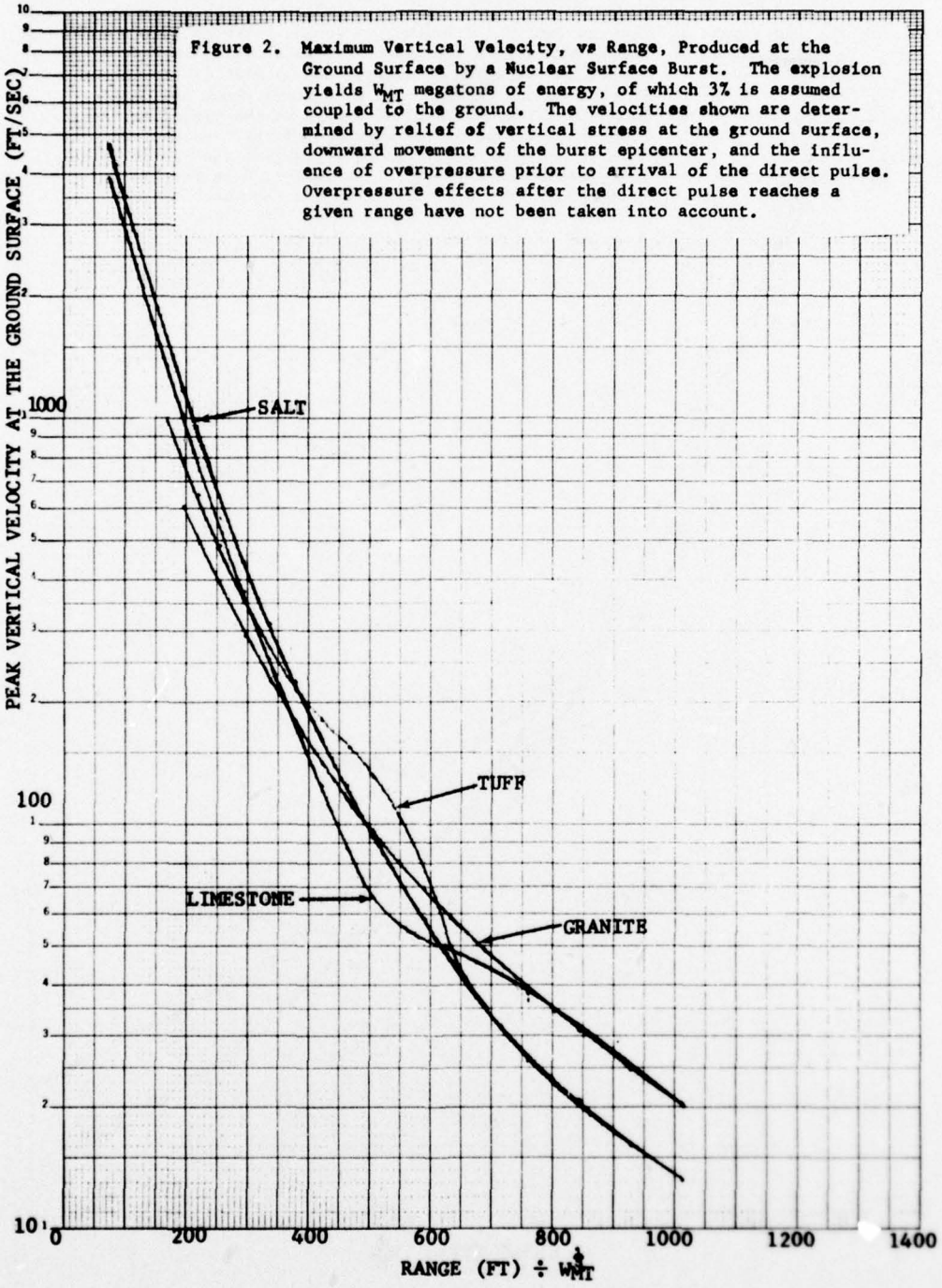

Figure 2. Maximum Vertical Velocity, vs Range, Produced at the Ground Surface by a Nuclear Surface Burst. The explosion yields W_{MT} megatons of energy, of which 3% is assumed coupled to the ground. The velocities shown are determined by relief of vertical stress at the ground surface, downward movement of the burst epicenter, and the influence of overpressure prior to arrival of the direct pulse. Overpressure effects after the direct pulse reaches a given range have not been taken into account.

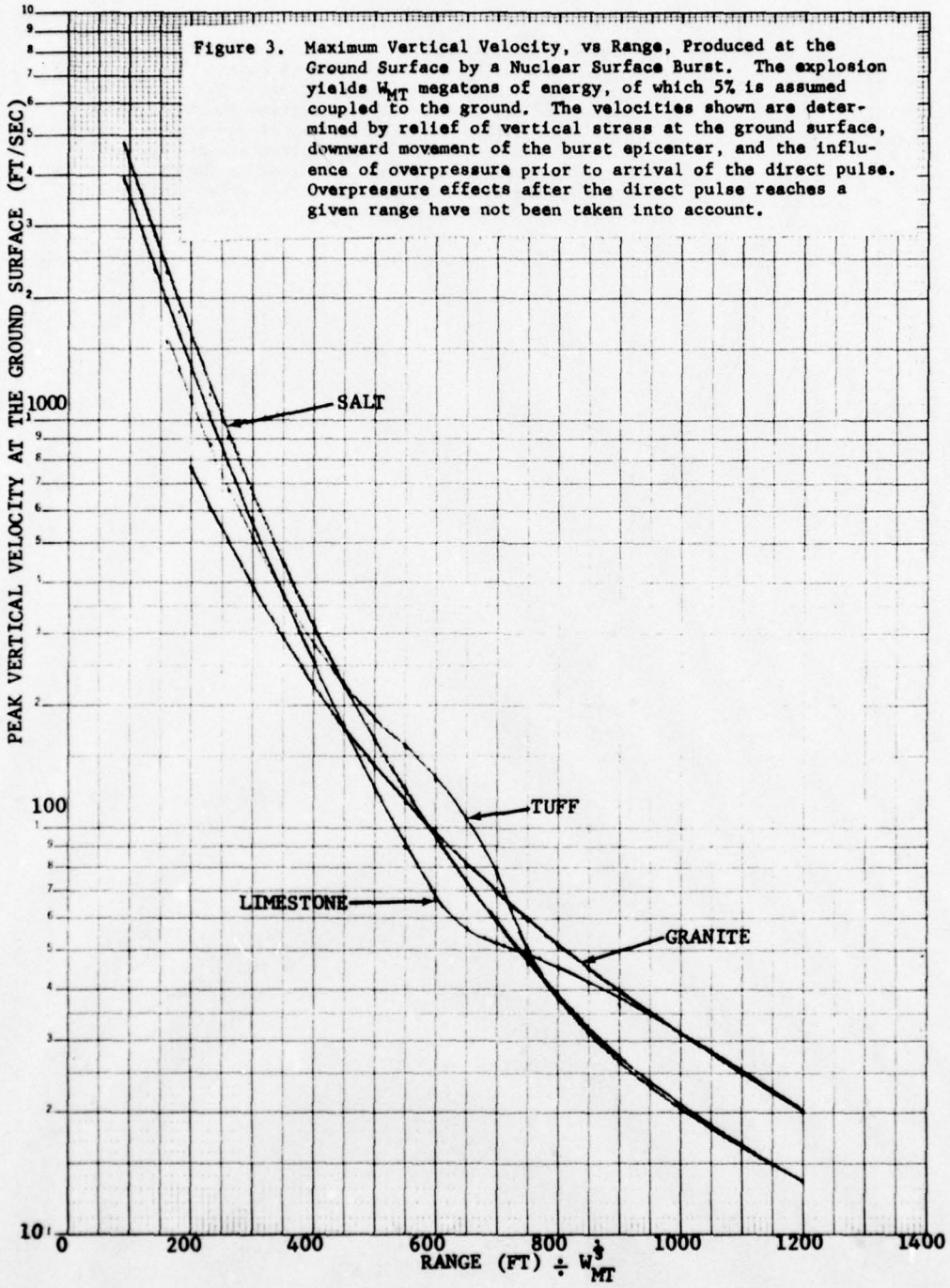

Figure 3. Maximum Vertical Velocity, vs Range, Produced at the Ground Surface by a Nuclear Surface Burst. The explosion yields W_{MT} megatons of energy, of which 5% is assumed coupled to the ground. The velocities shown are determined by relief of vertical stress at the ground surface, downward movement of the burst epicenter, and the influence of overpressure prior to arrival of the direct pulse. Overpressure effects after the direct pulse reaches a given range have not been taken into account.

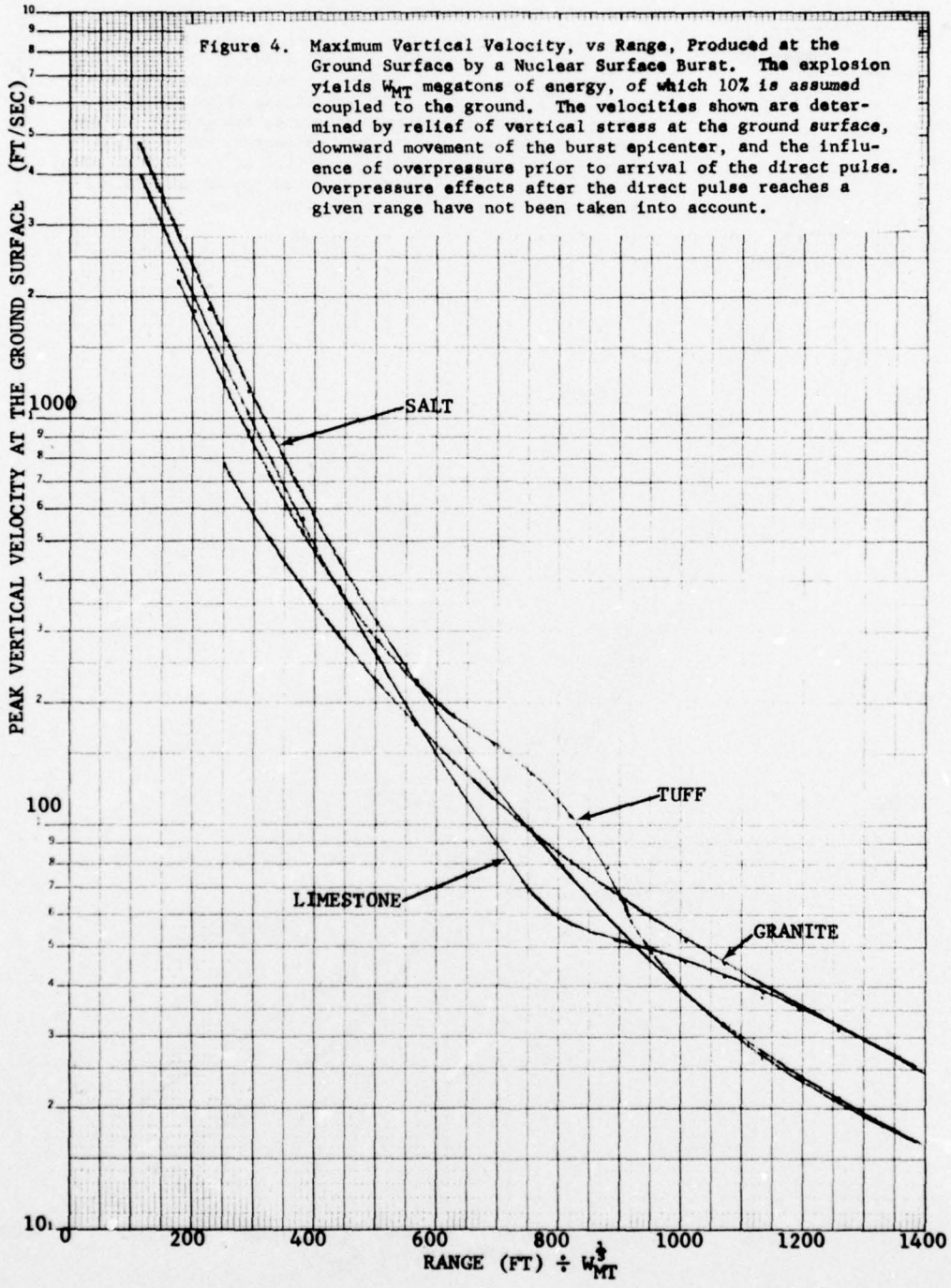

Figure 4. Maximum Vertical Velocity, vs Range, Produced at the Ground Surface by a Nuclear Surface Burst. The explosion yields W_{MT} megatons of energy, of which 10% is assumed coupled to the ground. The velocities shown are determined by relief of vertical stress at the ground surface, downward movement of the burst epicenter, and the influence of overpressure prior to arrival of the direct pulse. Overpressure effects after the direct pulse reaches a given range have not been taken into account.

Craters formed by ejection of material at the peak velocities shown in Figures 1 through 4 tend to be somewhat larger in radius - but not by much - than is predicted by present experimentally-based relations between yield and crater size. To reach such a conclusion even when no loss of coupled energy from ground material is permitted, must raise doubts regarding assumptions that are basic to present calculations of crater formation. More disquieting still is the observation that overpressure effects not included in Figures 1 through 4 have greatly retarded ejecta formation in past calculations. In Section 3, further attention is given to the meaning of the fact that the presumably overblown craters implied by Figures 1 through 4 are not much larger than observed craters. However, detailed discussion of the matter will await completion of the overall study.

An unexpected result was obtained for the final depth of the burst epicenter. Specifically, applying the definition of coupled yield-fraction suggested in Section 1.3.2, both the spherically-symmetric fields used in the present study, and axisymmetric fields calculated in past programs, give distances of epicenter migration that can be expressed within 10% as $8.7W_{KT}^{\frac{1}{3}}$ ft, where W_{KT} is the coupled energy in kilotons (1 kiloton (KT) = 4.186×10^{19} erg). To the limited extent that pertinent data are available, that result is independent of (a) the fraction of the yield coupled to the ground, (b) the depth of burial of the shot point, and (c) heat of vaporization, over the range 2.5×10^{10} erg/gm to 1.3×10^{11} erg/gm. In the case of tuff, however, with an air-void fraction of 5% and an assumed vaporization energy of 2.0×10^{10} erg/gm, the calculated change in epicenter depth was $13.3W_{KT}^{\frac{1}{3}}$ ft. If the result for tuff is included, then the average distance of epicenter migration becomes $9.3W_{KT}^{\frac{1}{3}}$ ft. To produce the curves of Figures 1 through 4, we

utilized final epicenter depths inferred from calculations of tamped bursts in each of the four individual media.

It was also found possible (as epxected) to compress into a simple formula cavity-size data obtained from many calculations of tamped bursts. In particular, for a tamped explosion of yield W_{KT}, the cavity radius, in feet, is usefully approximated by the expression $177\ W_{KT}^{\frac{1}{3}} Y_{VM}^{-2/7}$, where Y_{VM} is the von Mises limit of material strength, in bars. The expression noted holds within 15% for a wide range of calculations of tamped bursts in ground media. The data on which the formula is based include (a) variations in the von Mises limit of strength from ten bars up to at least a kilobar, (b) bulk moduli from 20 kilobars (kb) to 650 kb, and Poisson's ratios from .15 to .35, (c) non-ideal plasticity that corresponds roughly to a variation of the tangent of the angle of internal friction from .16 to 1.06, (d) air-void fractions from 0 to 5%, and (e) overburden stresses from 1 bar to 181 bars. The largest deviations from the simple formula arise in tuff, and result from compaction ("tuff"'s air-void-fraction is 5%); variations in the equation of state of vaporized ground material also cause significant deviations from the simple formula. Apart from its application here in obtaining a measure of the contribution of plastic flow to crater volume, the formula should prove useful in defining the effects of underground nuclear explosions.

It seems clear, yet not rigorously demonstrable, that the portion of the crater volume due to plastic flow of ground material must be less than half the volume of a cavity formed at an overburden of 1 bar in a tamped burst of yield $2W_{KT}$, if W_{KT} is the energy coupled in a surface burst. In addition, the total volumes of craters produced by nuclear surface bursts of interesting yield are presently estimated as 100-150 ft^3 per

ton of yield. We therefore conclude that Source 3 could generate a crater by plastic flow alone only in materials with von Mises limits of strength smaller than 264-424 psi: to account for ten percent of the crater volume by plastic flow, Y_{VM} would have to be smaller than 268-429 bars.

SECTION 2
RESULTS AND COMPUTATIONAL DETAILS

2.1 Peak Vertical Velocity, vs. Range: Uniaxial and Spherical Velocity Fields, and Their Superposition.

Under the rules of simple scaling, the dependence of intensive field variables (velocity, stress, etc.) on position, time, and yield can be expressed for all yields in terms of scaled position and time alone, where scaled position coordinates and scaled time are the actual coordinates and time, divided by the cube root of the energy that drives the motion. To bound the stresses and particle velocities created by energy deposition in the earth, we imagine a definite fraction α of the yield W released in a nuclear surface burst as residing in the ground below a rigid, perfectly reflecting air-ground interface, from a very early time onward - "early" relative to the time required to disturb all material on the crater region. The hemispherical field that would then develop in the ground is identical to that issuing from a tamped explosion in which the energy $2\alpha W$ is released, and we have therefore studied spherically-symmetric motions calculated in tuff, salt, granite and limestone. The scaled time and space variables on which the resulting spherical fields depend are denoted henceforth as $\hat{t}$ and $\hat{R}$, and are related to the actual time t, and distance R from the burst point, by the formulas

$$\hat{t} = t/(2\alpha W)^{\frac{1}{3}} \qquad (1)$$

$$\hat{R} = R/(2\alpha W)^{\frac{1}{3}} \qquad (2)$$

The field induced in the ground by the rest of the yield (i.e., the "airblast-induced" field) depends only on the space and time variables

$$\hat{t} = t[1-\alpha)W]^{\frac{1}{3}} \approx t/W^{\frac{1}{3}} \tag{3}$$

$$\hat{R} = R/[(1-\alpha)W]^{\frac{1}{3}} \approx R/W^{\frac{1}{3}} \tag{4}$$

As far as is known, most of the energy coupled to the ground during the rad-hydro phase of a nuclear surface burst is soon transferred to the fireball. As a result the "approximate" forms of Equations (3) and (4) (with $\approx$ symbols) are probably more accurate than the "exact" forms (with = signs). Moreover, the fraction α is small. Hence, the approximate forms of Equations (4) and (5) will be used hereafter. Equations (1) through (4) then imply that the scaled ranges and times $\hat{R}$, $\hat{t}$, $\widehat{R}$ and $\widehat{t}$ are related as follows:

$$\widehat{R} = \hat{R}/(2\alpha)^{\frac{1}{3}} \tag{5}$$

$$\widehat{t} = \hat{t}/(2\alpha)^{\frac{1}{3}} \tag{6}$$

Equations (1) through (6) specify in full how the equivalent radius-time coordinate systems (R,t), $(\widehat{R,t})$ and $(\hat{R},\hat{t})$ are related.

The hemispherical field that would develop below a rigid ground-surface plane from a source of coupled energy αW includes the variables $u_r(\widehat{R,t})$, $\sigma_\varphi(\widehat{R,t})$, $\rho(\widehat{R,t})$, $C_L(\widehat{R,t})$ and $\widehat{d_v}(\widehat{R,t})$, where d_v is the largest radius to which ground material vaporizes ($d_v=(2\alpha W)^{\frac{1}{3}}\widehat{d_v}$); u_r, σ_φ, ρ and C_L denote, respectively, radial particle velocity, azimuthal stress, density and the speed of propagation of ambient longitudinal loading waves. The airblast-induced field includes the vertical component of particle velocity at the ground surface, namely $U_v(\hat{R},\hat{t})$. At the three levels of approximation for which results have now been generated, the variables u_r, σ_φ, C_L, ρ, d_v and U_v furnish upper bounds to the maximum vertical velocity imparted to ground material at any given range, namely

$$U_{max}^{(1)} = \text{Maxt}(\sigma_\varphi/\rho C_L) \tag{7}$$

$$U_{max}^{(2)} = \text{Maxt}\left(\sigma_{\varphi}/\rho C_L + 2u_r d_v/\sqrt{d_v^2+R^2}\right) \tag{8}$$

$$U_{max}^{(3)} = \text{Maxt}\left(\sigma_{\varphi}/\rho C_L + 2u_r d_v/\sqrt{R^2+d_v^2} + U_v\right) \tag{9}$$

In Equations (7), (8) and (9), Maxt(F) denotes the maximum value attained by a field variable F as a function of time at a fixed range.

The velocity $U_{max}^{(1)}$ takes account only of stress relief at the ground surface as the direct-induced pulse runs past a specified range in the absence of overpressure. $U_{max}^{(2)}$ includes both the effects of stress relief, and downward migration of the burst epicenter, but again with zero overpressure. Stress relief, migration of the burst epicenter and overpressure are represented in $U_{max}^{(3)}$; overpressure-impulse propagates through ground material at the longitudinal loading-wave speed, giving rise to a minimal downward velocity increment.

In doubling the vertical component of radial particle velocity to obtain the contribution to $U_{max}^{(2)}$ from epicenter migration, [Equation (8)], we have ignored the fact that for oblique incidence of the direct pulse, the contribution of stress relief to the jump-off velocity of the ground surface is already partially accounted for by the term $\sigma_{\varphi}/\rho C_L$. Thus, the bound provided by Equation (8) has been raised somewhat in the interest of simplicity. For example, a shock normally incident on the ground surface from below would produce the quantity $(2u_r+\sigma_{\varphi}/\rho C_L)$ as the argument of Maxt in Equation (8); the correct result for an elastic material is $2u_r$. However, in view of the overestimate of peak vertical velocity implicit in Equation (8), the alternatives of rotating the stress tensor through $\theta(R)$, or of using exact results for the problem of oblique shock incidence at the free surface of an elastic medium, do not represent refinements of real interest. Equation (2) has also been simplified by

observing that $\sigma_\varphi/\rho C_L$ attains its maximum value at any given range at a time $t_{max}^{(1)}$ when u_r is very close to its maximum. Hence, the argument of Maxt in Equation (8) has simply been evaluated at the time $t_{max}^{(1)}$ in computing $U_{max}^{(2)}$.

In computing $U_{max}^{(3)}$, we have taken advantage of the fact that at time $t_{max}^{(1)}$ the airblast-induced field changes much more slowly near the ground surface than the direct-induced field. The time at which the right hand member of Equation (9) attains its maximum value is therefore almost identical to $t_{max}^{(1)}$. Simply-scaled for yield W, the time $t_{max}^{(1)}$ is designated $\hat{t}_{max}^{(1)}$ [Equation (6)]. Thus, we have equated $U_{max}^{(3)}$ to the value assumed by the righthand member of Equation (9) at a time $\hat{t}$ equal to $\hat{t}_{max}^{(1)}$. Furthermore, over propagation-distances of interest here (hundreds of feet), physical (i.e., unscaled) transit times of direct-induced pulses are not sensitive to α. Hence, having determined those times for a given medium with α equal to .05, the same transit times were assumed to apply to all values of α from .03 to .1; the transit-time errors incurred thereby are small (<15% for tuff, and <10% otherwise).

2.2 Ground Motion on the Crater Region: No Overpressure; Burst Epicenter Fixed at the Ground Surface

For tamped bursts in infinite tuff, salt, granite and limestone media, the peak azimuthal stress and peak radial particle velocity are shown in Table 1 at various ranges. In every case, the energy released by the explosions represented in the table is equal to 1 kiloton (KT) (4.184×10^{19} ergs). The time at which the peak azimuthal stress is attained is also shown for each range, as well as the acoustic impedance of material in the state of peak azimuthal stress.

From the data of Table 1, the jump-off velocity acquired by each material at a surface where its peak azimuthal stress is

TABLE 1.

VALUES OF PEAK AZIMUTHAL STRESS (σ_φ), IMPEDANCE ($\rho_o C$), AND PEAK RADIAL PARTICLE VELOCITY (u_r) AT VARIOUS DISTANCES FROM THE CENTER OF A 1-KILOTON TAMPED SPHERICAL BURST. The Time at Which Peak Values are Reached is Also Shown at Each Range. Data are Presented for Granite, Limestone, Salt and Tuff, the Four Materials Studied. The Units of Length, Mass and Time for the Tabulated Variables are Centimeters (cm), Grams (gm) and Milliseconds (ms), Except that Ranges are Given in Feet.

GRANITE

Range (ft)	σ_φ (kb)	$\rho_o C$ (gm/cm²/ms)	u_r (cm/ms)	Time (ms)
49	23.40	1570	26.6	2.0
84	7.75	1260	11.8	4.0
116	4.03	1260	6.1	6.0
145	2.49	1100	4.0	8.0
172	1.66	1100	2.8	10.0
200	1.16	1100	2.5	12.0
227	0.83	1100	1.8	14.0
253	0.68	1100	1.4	16.0

LIMESTONE

Range (ft)	σ_φ (kb)	$\rho_o C$ (gm/cm²/ms)	u_r (cm/ms)	Time (ms)
25	90.	1230	70.3	1.0
38	24.	1070	27.2	2.0
50	18.	1070	20.3	3.0
63	12.	870	16.0	4.0
73	9.5	870	11.7	5.0
84	6.7	870	8.9	6.0
94	4.7	870	6.9	7.0
103	3.5	810	5.5	8.0
113	2.6	930	4.5	9.0
124	1.89	930	3.8	10.0
138	1.33	910	3.1	11.0
151	1.31	910	2.9	12.0
161	1.21	910	2.9	13.0
172	1.11	910	2.7	14.0
184	1.05	910	2.4	15.0
196	0.98	910	2.2	16.0
204	0.84	910	2.0	17.0
218	0.82	910	1.8	18.0
227	0.75	910	1.6	19.0
237	0.66	910	1.6	20.0

TABLE 1. (Continued)

SALT

Range (ft)	σ_∞ (kb)	$\rho_o C$ (gm/cm²/ms)	u_r (cm/ms)	Time (ms)
19	147	1366		.68
21	128	1340	117	.75
28	74	1300	76	1.23
30	66	1258	70	1.38
38	43	814		2.01
66	11.3	792	14.3	4.4
95	5.3	792		6.8
102	4.2	792	5.9	7.4
127	2.38	792	3.5	9.7
134	1.99	800	3.0	10.4
190	0.73	870		14.7
199	0.66	880	1.24	15.6
209	0.60	916	1.16	16.2
240	0.44	1007	.91	18.4
274	0.38	1050	.74	20.6

TUFF

Range (ft)	σ_∞ (kb)	$\rho_o C$ (gm/cm²/ms)	u_r (cm/ms)	Time (ms)
8.5	652	3300	436	.15
12.9	200	2000	210	.37
18.1	90	798	127	.74
22.8	54	655	83	1.10
27	35	587	62	1.47
30	23.9	538	48	1.84
45	10.2	408	27	3.7
58	6.6	341	16.9	5.5
68	4.1	290	11.5	7.4
83	1.99	224	7.5	11.0
97	1.07	188	4.4	14.7
107	.84	157	3.6	18.4
116	.68	136	3.5	22.1
123	.54	126	2.82	26
131	.45	126	2.31	30
142	.41	138	1.95	33
154	.34	160	1.39	37
163	.31	223	1.25	44
214	.200	299	.73	52
258	.128	420	.49	59

instantaneously and completely relieved, has been computed as a function of range. For reasons stated above (Section 1.3.3), the resulting particle velocities are almost certainly considerably larger than the maximum vertical velocities attained at the same ranges in a surface burst in which ½ KT of energy is coupled to the ground. For surface bursts of arbitary yield in which 3%, 5%, 8% and 10% of the yield becomes coupled to the ground, corresponding overestimates of peak vertical velocity are found as functions of range by direct application of the rules of simple scaling. Specifically, if the yield of the device, in megatons, is denoted W_{MT}, then the coupled energy, in kilotons, is equal to $1000\alpha W_{MT}$. The variables σ_φ, etc, of the direct-induced field on which the upper-bound velocity $U_{max}^{(2)}$ is based, are then obtained for a tamped spherical burst yielding $2000\alpha W_{MT}$ kilotons of energy. Now, $\sigma_\varphi(R,t)$ etc, refer to the values of intensive field variables at range R from a 1-KT burst, and at time t after release of the yield of 1 KT (Table 1). Hence, $\sigma_\varphi(R/(2000\alpha W_{MT})^{\frac{1}{3}}, t/(2000\alpha W_{MT})^{\frac{1}{3}})$, etc, represent the azimuthal stress, etc, at range R and time t from a tamped burst whose yield, in KT, is $2000\alpha W_{MT}$. If all distances and times are simply-scaled with respect to the yield W_{MT}, then we find from Equations (3) and (4) that the azimuthal stress is given by $\sigma_\varphi(\hat{R}/(2000\sigma)^{\frac{1}{3}}, \hat{t}/(2000\alpha)^{\frac{1}{3}})$, etc.

For the coupling fraction .05, the upper-bound vertical velocities estimated from Equation (6) are plotted as functions of range in Figure 5. The plot is in log-log format, so that curves appropriate to coupled fractions .03, .08 and .1 are identical to the curve shown except for simple translations to the left and right, through distances that correspond to uniform changes in the scale of range by the factors $(3/5)^{\frac{1}{3}}$, $(8/5)^{\frac{1}{3}}$ and $2^{\frac{1}{3}}$, respectively.

2.3 Ground Motion on the Crater Region: No Overpressure; Burst Epicenter Below the Ground Surface

The depth to which the burst epicenter migrates in the

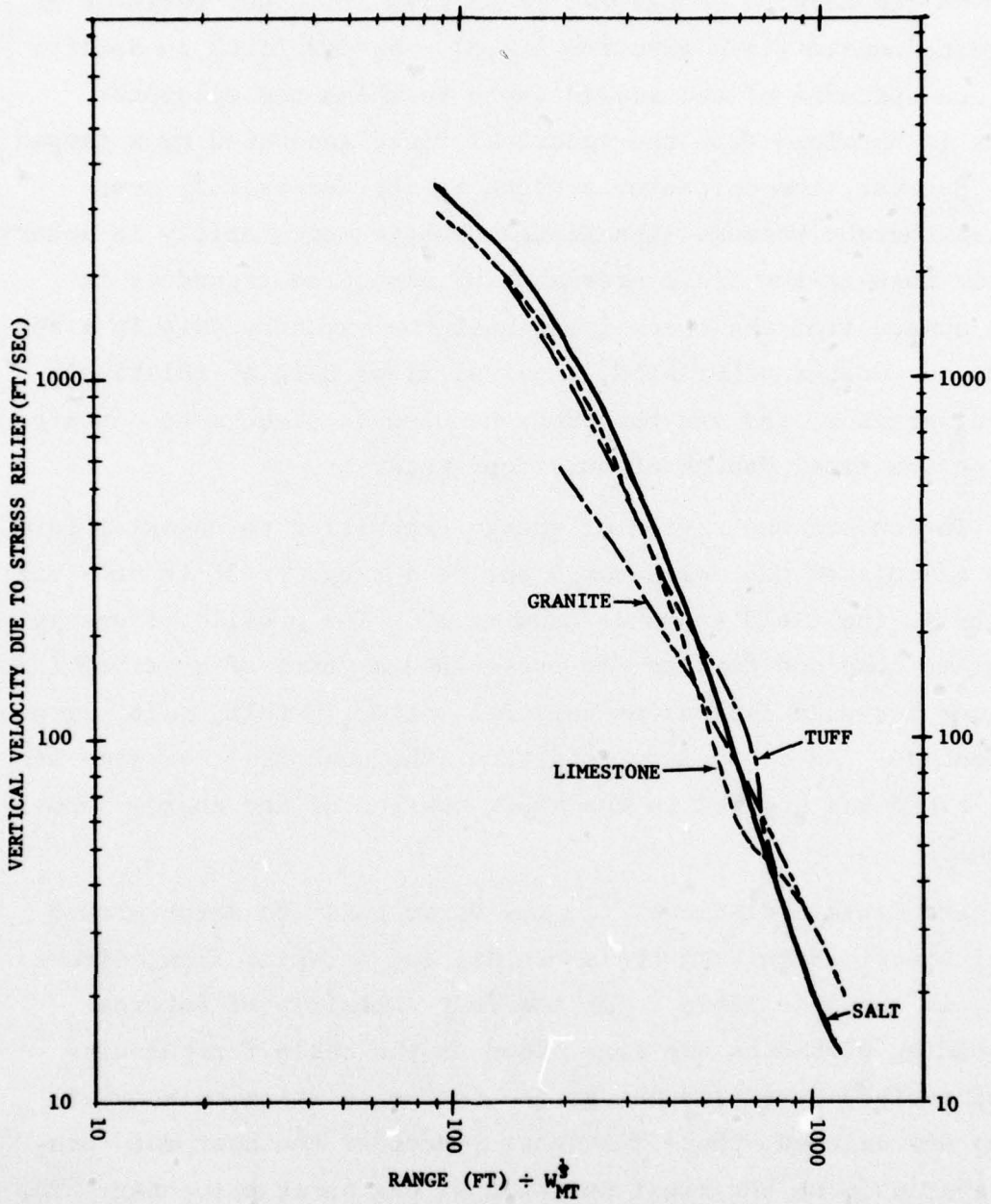

Figure 5. Vertical Velocity Imparted to Near-Surface Ground Material by Relief of Stress in a Horizontally-Propagating Pulse. The pulse is created by a nuclear surface burst yielding W_{MT} megatons of energy, of which the fraction .05 is assumed coupled to the ground.

course of a nuclear burst is considered simply-scalable with respect to the coupled energy αW, along with all other features of the direct-induced field (Section 1.3.2). As described in Section 1.3.3, one estimate of the scaled depth to which the epicenter migrates is obtained from the spherical field generated by a tamped burst. However, the epicenter's depth is not necessarily overestimated thereby because streamlines diverge more rapidly in spherical flow than in the field presented by vaporized ground as it expands upward from the shock front near the symmetry axis in a surface burst. On the other hand, uniaxial flows display relatively little divergence, and can therefore be used to place more certain bounds on the final depths of burst epicenters.

To convert the region of energy deposition to uniaxial form, we have calculated the mean energy out to a range of 26 ft at a variety of depths in the field known as "Source 3". The profile of energy per unit volume obtained thereby was prescribed as part of a set of initial conditions for calculations of uniaxial motion in tuff, salt, granite and limestone. As a boundary condition, the canonical overpressure at zero range was applied to the upper surface of the energy deposition region.

The maximum distance from the burst point to which ground material vaporized in both the spherical and uniaxial flow calculations, is shown in Table 2 for the four materials of interest. Corresponding distances are also shown in the table for calculations of surface-burst-induced ground motion in which only axial symmetry was assumed; those distances represent the best data presently available on the final position of the burst epicenter. The main facts exhibited by Table 2 are that (a) all scaled depths other than those obtained in uniaxial approximation are for practical purposes identical, and (b) the depths obtained when uniaxial motion of vaporized and solid ground is assumed, exceed all other depths, as expected. The result (a) can be accounted for partly as the

TABLE 2.

DEPTHS THROUGH WHICH THE EPICENTER SINKS IN TAMPED NUCLEAR EXPLOSIONS AND NUCLEAR SURFACE BURSTS. Depths are Expressed in Feet. For Surface Bursts, a Kiloton of Energy is Assumed to be Coupled to the Ground; For Tamped Explosions the Yield is Two Kilotons. All the Tamped Explosions Listed have Spherical Symmetry, and Vice Versa.

		GROUND MEDIUM AND HEAT OF VAPORIZATION (erg/gm)			
SYMMETRY OF FIELD	SPECIAL REMARKS	SALT (1.3×10^{11})	GRANITE (3.5×10^{10})	LIMESTONE (2.5×10^{10})	TUFF (2.0×10^{10})
Spherical		7.78	7.79	8.69	13.3
Uniaxial	Simulates Source 3	19.7	33.4	30.0	42.1
Axisymmetric	Buried at $\frac{1}{3}$ 15 ft/MT		9.5		
Axisymmetric	Source 0		7.8		
Axisymmetric	Source 2		9.8		

result of a cancellation of two opposed errors (excessive divergence, but no loss of energy), partly as a result of the restricted range of vaporization energies presented by the solids studied (from 2×10^{10} erg/gm for tuff to 1.3×10^{11} erg/gm for salt), and partly as a result of a rapid decay of shock pressure with depth that tends to minimize the variation of epicenter depth with heat of vaporization. Doing away with streamline divergence leads to result (b); relative to the final epicenter depths reached in the other calculations of Table 2, calculations in which uniaxial flow is assumed show increases in epicenter depth by factors of 2.5 (in granite) to 4.2 (in salt).

From the calculations of axisymmetric and spherically-symmetric motion represented in Table 2, epicenter depths are given in feet by the expression $9.3(\alpha W)^{\frac{1}{3}}$ for near-surface bursts, where the yield W is expressed in kilotons and α retains its meaning as the fraction of the energy coupled. By assuming motion near the symmetry axis to be vertical and uniaxial, an upper bound to the epicenter's depth is obtained that runs from $24(\alpha W)^{\frac{1}{3}}$ (for salt) to $39(\alpha W)^{\frac{1}{3}}$ (for granite). For present purposes, however, the main fact conveyed by the data of Table 2 is the following: In all cases, the lines joining the epicenter to the ground-surface points of major interest make angles $\theta(R)$ with the horizontal that are too small to add a significant upward component of particle velocity to the upward velocity resulting from stress relief.

Since we find that burst-epicenter migration in surface bursts adds no more than about 10% to the peak vertical velocities of surface material, the upward component of particle velocity (the peak radial particle velocity multiplied by $\sin\theta(R)$) has been plotted by itself in Figure 6; the changes to Figure 5 produced by adding the velocities of Figure 6 to those of Figure 5 are inconsequential. As in Figure 5, curves appear only for a coupled-energy-fraction

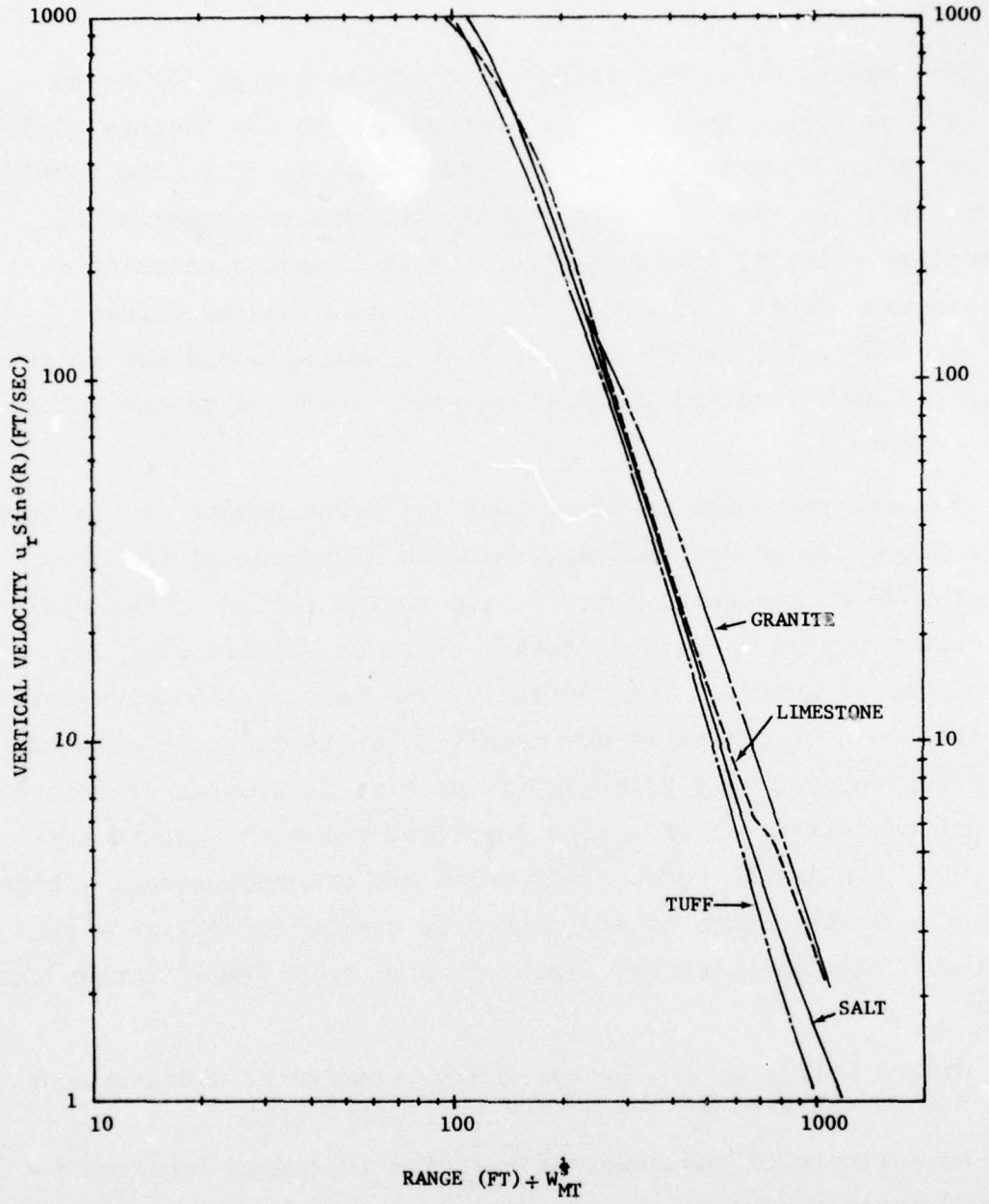

Figure 6. Vertical Component of Velocity Imparted to Near-Surface Ground Material as a Result of Downward Migration of the Epicenter of a Nuclear Surface Burst. Material just below the surface receives a positive vertical increment of velocity, whose maximum is shown here, on being disturbed by the pulse that radiates from the epicenter; subsequent relief of stress at the surface further increases the upward velocity of surface material (Figure 4). $\theta(R)$ denotes the angle made with the horizontal by a radial line from the epicenter to the ground surface at range R; u_r is the peak particle velocity produced at R by the direct wave along that line. The explosion yields W_{MT} megatons of energy, of which the fraction .05 is assumed coupled to the ground.

α, of .05. Again, a uniform translation of the curves for α=.05 to the left or right, by distances appropriate to the factors $(3/5)^{\frac{1}{3}}$, $(8/5)^{\frac{1}{3}}$ and $2^{\frac{1}{3}}$, respectively, yields curves that apply to the coupled fractions .03, .08, and .1. Also, while the upward component of peak particle velocity shown in Figure 5 was computed assuming a final epicenter depth of $9.3(\alpha W)^{\frac{1}{3}}$ ft, even the bounding values $24(\alpha W)^{\frac{1}{3}}$ ft (for salt) and $39(\alpha W)^{\frac{1}{3}}$ ft (for granite) would not greatly increase the peak vertical particle velocity relative to the values shown in Figure 5.

Several years ago we found that for burst points just a short distance below the ground surface, downward migration of the burst epicenter made an important contribution to the motion of material on the crater region.[2] Evidently that state of affairs does not hold for surface bursts. Interestingly, the increase in epicenter depth with depth of burial is due mainly to an increase in coupled-energy-fraction, and only slightly (if at all) to greater efficiency, for ground vaporization, of energy deposited below the ground surface. Thus, for a 1-MT burst 15 ft below the ground surface - which is about the scaled depth of the center of Johnny Boy device - the calculated change in epicenter depth amounted to $9.5(\alpha W)^{\frac{1}{3}}$ rather than $9.3(\alpha W)^{\frac{1}{3}}$.

2.4 Ground Motion on the Crater Region, Including Overpressure and Downward Migration of the Burst Epicenter

An estimate of the downward velocity increment imparted to the ground by overpressure can be obtained from calculations of uniaxial vertical motion. In a series of calculations of that kind, the canonical overpressure was imposed as a function of time on the ground surface at each of several ranges, with the ground medium otherwise undisturbed. For granite, the resulting particle velocities at the ground surface are listed in Table 3 as functions of time at various ranges; ranges and times are expressed as the simply-scaled

TABLE 3.

DOWNWARD VELOCITY U_v INDUCED BY OVERPRESSURE FROM A SURFACE BURST AT THE SURFACES OF FOUR GROUND MEDIA, AS FUNCTIONS OF SCALED TIME $\hat{t}$ AND RANGE $\hat{R}$. $\hat{R}$ and $\hat{t}$ are Equal to Actual Ranges and Times in Feet (ft) and Milliseconds (ms), Divided by $W_{MT}^{1/3}$, where W_{MT} is the Yield in Megatons (MT). The Units of U_v are Feet per Second (ft/sec). The Ground Media are Assumed to be Disturbed Only by Overpressure-Induced Waves.

Medium \ Range $\hat{R}$ ($ft/MT^{1/3}$)	250		500		750		1000	
GRANITE	$\hat{t}$ ($ms/MT^{1/3}$)	U_v (ft/sec)	$\hat{t}$	U_v	$\hat{t}$	U_v	$\hat{t}$	U_v
	0.67	0	4.6	0	12.7	0	26.1	0
	1.88	67.	6.5	18.7	15.9	7.5	30.1	4.0
	4.0	34.	9.8	10.7	21.4	4.3	36.4	2.59
	6.1	22.3	13.2	7.7	27.3	3.2	42.3	1.99
	8.4	16.3	16.5	6.0	32.9	2.54	48.1	1.68
	10.6	11.8	19.9	4.8	38.6	2.10	54.0	1.45
	12.0	9.0	23.3	4.1	43.7	1.83	59.8	1.28
			26.7	3.5	47.3	1.65	63.7	1.22
			28.4	3.3			67.3	1.13
LIMESTONE	$\hat{t}$ ($ms/MT^{1/3}$)	U_v (ft/sec)	$\hat{t}$	U_v	$\hat{t}$	U_v	$\hat{t}$	U_v
	0.67	0	4.6	0	12.7	0	26.1	0
	2.23	86.	6.9	18.6	16.3	7.7	30.6	4.2
	5.1	35.	10.9	9.9	22.9	4.4	37.7	2.66
	8.1	18.9	14.9	6.9	29.4	3.2	44.3	2.04
	11.2	12.1	18.9	5.2	36.0	2.52	50.9	1.71
	14.2	9.1	22.9	4.2	42.5	2.08	57.5	1.50
	17.2	6.3	26.9	3.5	49.1	1.76	64.2	1.30
	17.9	5.5	30.9	2.95	55.6	1.53	70.8	1.18
			35.0	2.55	62.2	1.34	77.4	1.03
			39.0	2.26	62.4	1.12	84.1	.94
			40.4	2.17			84.4	.93

TABLE 3 (continued)

Medium \ Range R (ft/MT$^{\frac{1}{3}}$)	250		500		750		1000	
	$\hat{t}$ (ms/MT$^{\frac{1}{3}}$)	U_v (ft/sec)	$\hat{t}$	U_v	$\hat{t}$	U_v	$\hat{t}$	U_v
SALT	0.67	0	4.6	0	12.7	0	26.1	0
	2.18	111	6.5	24.5	15.7	9.2	30.0	4.6
	4.7	54	9.8	14.3	21.1	5.5	36.0	2.97
	7.3	34	13.1	10.7	26.5	4.1	41.7	2.30
	9.9	23.6	16.3	8.6	31.8	3.4	47.4	1.93
	12.4	17.3	19.6	7.2	37.2	2.86	53.0	1.67
	15.0	13.2	22.9	5.9	42.5	2.45	58.7	1.44
	17.6	10.4	26.2	5.1	47.9	2.14	64.3	1.34
	20.1	8.4	29.4	4.6	50.0	2.04	70.0	1.23
			32.7	4.1	57.6	1.78	75.6	1.11
			36.0	3.6	58.6	1.74	79.5	1.06
			37.3	3.5	59.7	1.68		
	$\hat{t}$ (ms/MT$^{\frac{1}{3}}$)	U_v (ft/sec)	$\hat{t}$	U_v	$\hat{t}$	U_v	$\hat{t}$	U_v
TUFF	0.67	0	4.6	0	12.7	0	26.1	0
	2.66	285	7.2	107	17.0	21.0	31.5	9.1
	6.3	158	11.4	53	24.5	11.1	40.9	5.8
	9.7	127	15.7	32	32.1	8.3	49.3	4.6
	13.0	110	20.0	23.4	39.7	7.0	57.8	3.9
	16.3	87	24.3	19.1	47.3	6.0	66.2	3.3
	19.7	74	28.6	15.3	54.9	5.2	74.7	2.90
	23.1	64	32.9	12.6	62.5	4.6	83.2	2.64
	26.4	55	37.2	10.8	70.1	4.2	91.6	2.41
	29.8	44	41.5	9.6	77.7	3.8	100.1	2.15
			45.8	8.5	85.3	3.4	108.6	2.14
			50.1	7.4	92.9	3.13	113.8	2.01
			54.4	6.6	98.0	2.93		
			58.7	6.4				
			63.0	5.7				
			67.3	5.7				
			71.6	5.2				
			75.9	5.1				

variables $\hat{R}$ and $\hat{t}$ (Equations (3) and (4)), with the yield W in megatons. Corresponding results for limestone, salt and tuff are also presented in Table 3. From the data of Table 3, the downward velocities imparted to ground material by overpressure can be found at the times when direct-induced motions of maximum amplitude occur at a variety of ranges along the ground surface. For that purpose the times $t_{max}^{(1)}$ of Table 1 are converted to times $\hat{t}_{max}^{(1)}$ by means of the multiplicative factor $(2000\alpha)^{\frac{1}{3}}$. The overpressure-induced vertical velocity at the range-dependent time $t_{max}^{(1)}$, namely $U_v(R,t_{max}^{(1)})$, has been plotted in Figure 7 vs. R, for each of the four materials studied. As in the case of epicenter migration (Section 2.3), we also find that the increment in vertical velocity due to overpressure is not significant relative to that due to relief of direct-induced stresses (Section 2.2; Figure 5).

It should be clearly understood that the data of Table 3 and Figure 7 represent only a small portion of the total downward velocity imparted by overpressure to near-surface material when ejecta craters are produced by nuclear surface bursts. In particular, only the downward velocity attained up to the time when ejecta formation begins is represented in Figure 7 and its source data. For reasons outlined in Section 1.3.7, downward velocities induced by overpressure in disintegrating near-surface ground material are expected to be 10 to 100 times larger than those of Figure 6. However, the final phase of the present study, which is directed to overpressure effects on cracked ground material, has not been completed.

The curves of Figures 1 through 4, which convey the overall results generated to date in the program reported here, are obtained by simple addition, after scaling, of the velocities depicted in Figures 5, 6 and 7.

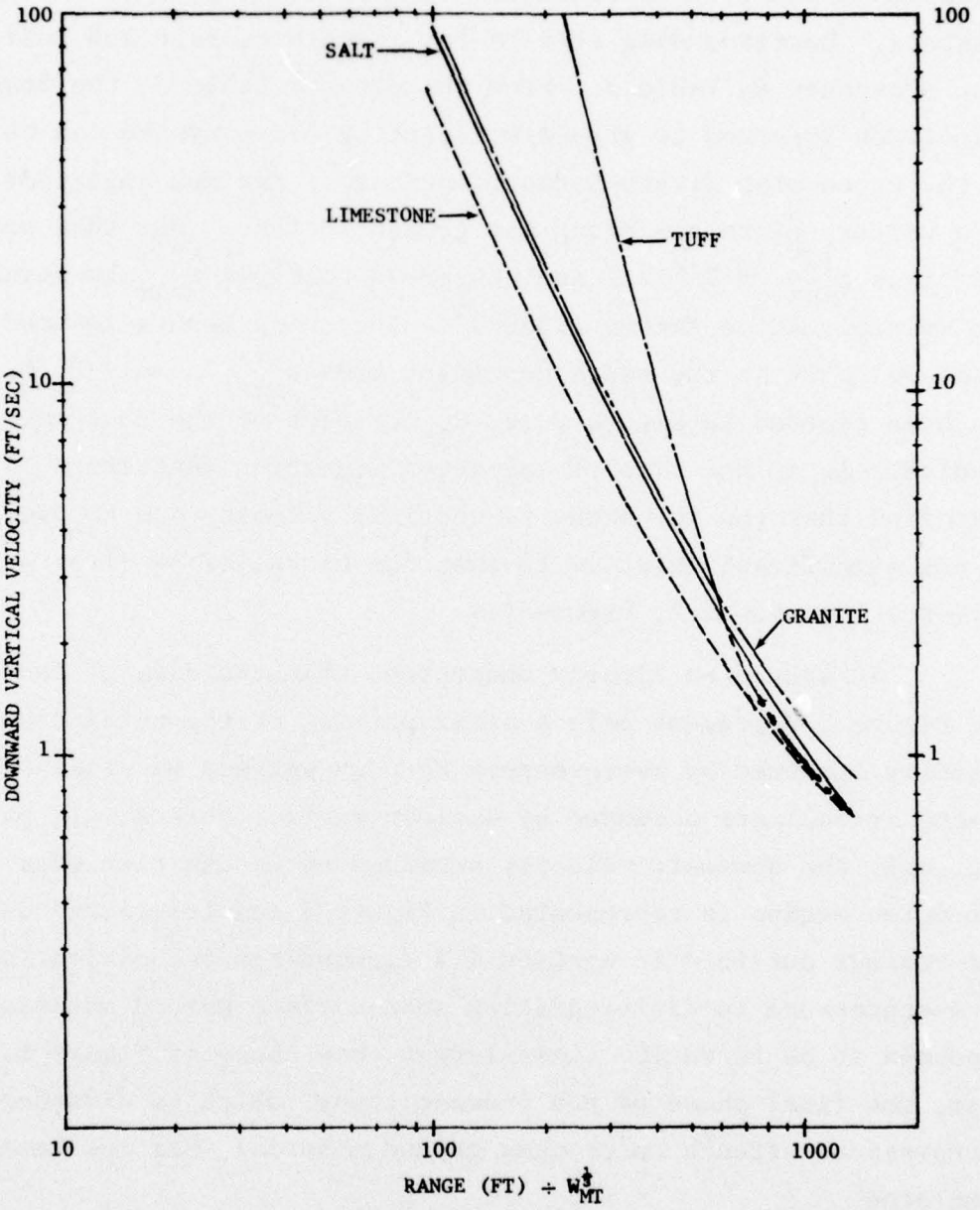

Figure 7. Downward Vertical Velocity Imparted to Continuous Ground Media by Overpressure from a Nuclear Surface Burst. W_{MT} is the yield of the burst in megatons.

2.5 Contribution of Plastic Flow to Crater Volume

Many calculations have been made of tamped nuclear bursts in geologic materials, in which the mechanical properties of the materials have been subjected to wide variations. Results of such calculations are shown in Figure 8, where the cavity radius is plotted as a function of time for a variety of salt media; both the radius and time are simply scaled to a yield of a kiloton in Figure 8. The most elaborate model of salt represented in Figure 8 includes the effects of (a) shear failure as described by a combined Mohr-Coulomb and von Mises yield surface, and associated flow rule, (b) collapse of air-void space with consequent hysteretic changes in the volume of material, (c) a regime of generally nonlinear elastic behavior, (d) decreasing strength and shear modulus with increasing temperature, with strength falling to zero at the melting point, (e) thermal expansion of condensed material, and (f) a contribution to mean stress from vaporized salt that varies from 0% in condensed material to 100% in vapor states that cover a wide range of densities and temperatures.

The curves of Figure 8 refer to a salt medium at a uniform hydrostatic overburden of 1 bar. The main message of Figure 8 is that among all the paraphernalia of the full constitutive model, only the von Mises limit of strength and the pressure-volume-internal energy relation for vaporized material, play a major role in determining the sizes of cavities produced by tamped bursts. Specifically, with salt described as an elastic ideally-plastic material with a polytropic vapor phase, the calculated cavity had a final radius that differed by less than 10% from the radius obtained using the full-blown constitutive model. Furthermore, the cavity radius proved quite insensitive to variations in elastic moduli, and only moderately sensitive

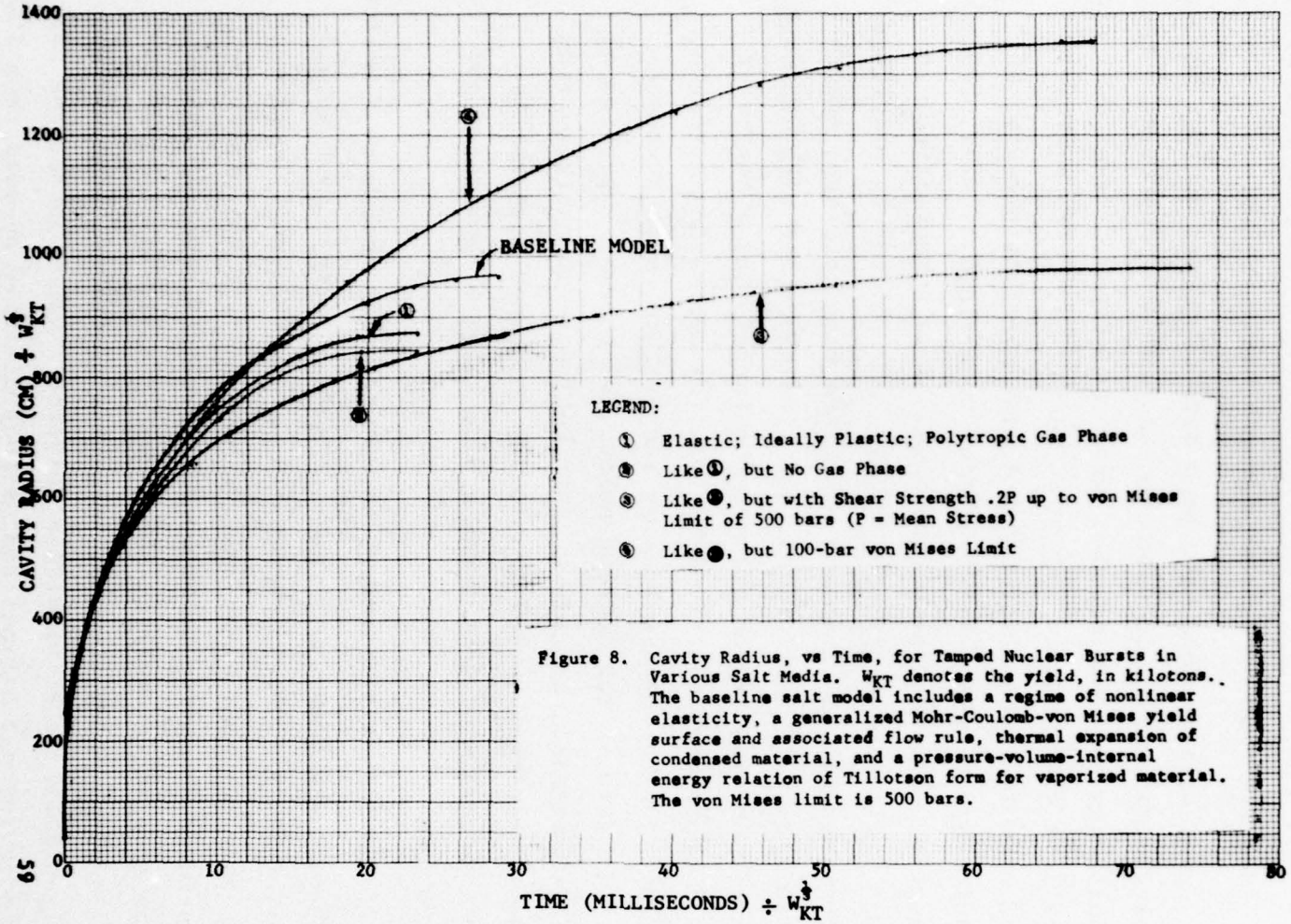

Figure 8. Cavity Radius, vs Time, for Tamped Nuclear Bursts in Various Salt Media. W_{KT} denotes the yield, in kilotons. The baseline salt model includes a regime of nonlinear elasticity, a generalized Mohr-Coulomb-von Mises yield surface and associated flow rule, thermal expansion of condensed material, and a pressure-volume-internal energy relation of Tillotson form for vaporized material. The von Mises limit is 500 bars.

to variations in the effective heat capacity ratio (commonly denoted "γ") - the characteristic parameter of the pressure-volume-internal energy relation. Overburden variations from 1 bar to 181 bars also had little effect on the cavity radius. However, as Figure 8 shows, variations of the von Mises limit of strength produce large changes in cavity radius in salt.

The simplified constitutive equations for salt contain few parameters, while the detailed equations encompass the full array of phenomena incorporated into "advanced" constitutive models. Hence, behavior similar to that of salt was anticpated for almost any geologic material. We verified that hypothesis for limestone and tuff, with one qualification: Extreme variation of the irreversible volume changes produced by loading and unloading the tuff medium, with its large air-void-fraction (~5%) led to an overall variation of 25% in calculated cavity radius;[9] however (Section 1.1), compaction craters are of little interest here. Granite, on the other hand, did not follow the example of salt. The von Mises limit of 20 kb ascribed to granite was much greater than that of salt, tuff or limestone, and could only be attained at mean-stress values of 40 kb or more. Since pressures fall below 40 kb in any cavity at an early stage of its growth, the final cavity radius was not determined by granite's von Mises limit. Rather, cavity growth was governed in granite by the rate of increase of strength with mean stress.

The results just discussed make it possible to write an approximate expression for cavity volume in terms of explosive yield and von Mises strength alone. In particular, we find that for 1 bar of overburden, the cavity volume V_c produced by a tamped burst of yield $2\alpha W_{MT}$ can be expressed within ±20% for limestone, salt and tuff by the relation

$$V_c = .046 \times 10^6 \, \alpha W_{MT} (10^7/Y_{VM})^{6/7} \qquad (10)$$

where Y_{VM} is von Mises' limiting value for the square root of the second invariant ($\frac{1}{2}\sigma'_{ij}\sigma'_{ij}$) of the deviatoric stress-tensor σ'_{ij}; the units of V_c, W_{MT}, and Y_{VM} are cubic feet, megatons, and bars respectively. We now recall (Section 1.3.8) that the volume V_c is due almost entirely to plastic flow, and that $\frac{1}{2}V_c$ should exceed by a substantial factor the portion of the total crater volume due to plastic flow in a nuclear surface burst of yield W_{MT}, in which the yield-fraction α becomes coupled to the ground. Hence, if V_{PF} denotes the plastic-flow-derived part of the total crater volume, we find that

$$V_{PF} < 0.023\times10^{6}\alpha W_{MT}(10^{7}/Y_{VM})^{6/7} \qquad (11)$$

$$Y_{VM} < 1.2\times10^{12}(\alpha W_{MT}/V_{PF})^{7/6} \qquad (12)$$

According to current experimentally-based estimates, the volume of the crater formed in a nuclear surface burst should lie within the range 100-150 ft^3 per ton of yield. Hence to account for the crater volume by plastic flow alone, W_{MT}/V_{PF} would have to assume a value between $(2/3)\times10^{-8}$ and 10^{-8} MT/ft^3. Equation (12) then implies that Y_{VM} must be smaller than 23.6 to 38 bars if α=.1, 10.5 to 17 bars if α=.05, and 5.6 to 9.0 bars if α=.03. For the currently popular Source 3, α has a maximum value of .08, and Y_{VM} would have to be smaller than 29.2 bars (424 psi) if 100 ft^3 of crater volume are to be produced by plastic flow per ton of yield, or smaller than 18.2 bars (264 psi) to produce a volume of 150 ft^3 per ton. To account for 10% of the crater volume by plastic flow would require a von Mises limit smaller than 347 to 557 bars for α=.1, 155 to 248 bars if α=.05, and 82 to 132 bars if α=.03; for Source 3, a volume of 10 ft^3 per ton of yield can result from plastic flow if Y_{VM} is smaller than 429 bars (6225 psi), or 15 ft^3 per ton if Y_{VM} is smaller than 268 bars (3880 psi).

2.6 Crater Depth

For materials whose von Mises limits of strength do not exceed a few kilobars, the radius of the hemisphere whose volume is given by the right-hand member of Equation (11) provides an estimate of the depth of the crater at its center. On that basis, crater depths of 129, 157 and 228 ft/MT$^{\frac{1}{3}}$ would be produced respectively, in limestone, salt and tuff by Source 3 (α=.08); respective values of Y_{VM} for those materials are 1000, 500 and 134 bars. As already noted, Equation (11) does not apply to granite, with its von Mises limit of 20 kb. Rather, the calculated cavity volume is determined for tamped bursts in granite by the generalized Mohr-Coulomb portion of the material's yield surface; from such calculations we obtain a crater depth of 88 ft/MT$^{\frac{1}{3}}$ for a surface burst that produces Source 3 in granite. However, for reasons noted in Section 1.3.8, the depths obtained from calculations of tamped bursts are not necessarily greater than would be produced by Source 3 below ground zero in the four half-spaces considered.

A bound on crater depth can be found by appeal to ejecta production, rather than to the plastic flow mechanism represented in Equation 11. In particular, if a fragment of ground material at a given range starts its flight with a vertical component of velocity equal to the upper-bound-value of Section 2.3, then the maximum height to which the fragment can rise in the earth's gravitational field sets a limit on the depth of the crater at that range. From Figure 1, for example, the peak vertical velocity at the surface of a granite half-space is 140 ft/sec at a range of 500 ft from a 1-MT surface burst in which 5% of the yield is coupled. In simple ballistic flight, a particle starting on a trajectory with that vertical component of velocity will increase its altitude by 306 ft before it begins to fall. With decreasing range the limiting depth so derived increases to much larger values still. Thus, the simple limit of maximum ejecta

altitude tends to give a gross overestimate of crater depth, especially at smaller ranges, a result that stems principally from neglect of two factors. In the first place, during the time taken by a release wave from the ground surface to reach a depth equal to the maximum ejecta altitude at a given range, $\sigma_\varphi/\rho C$ falls below its peak value. Secondly, in the same period of time and at that same depth, an appreciable downward velocity increment will also have been imparted to material by the direct pulse. Hence, a more useful estimate of the crater depth d_c, and probably still an upper bound, would be obtained by solving the following equations for the variable $\hat{d}$:

$$\hat{t} = \hat{d}/\overline{C} + \hat{t}^{(1)}_{max} \tag{13}$$

$$u_v = \sigma_\varphi(\hat{r},\hat{t})/\rho_o\overline{C} - u_r\hat{d}/\hat{r} \tag{14}$$

$$\hat{d} = \begin{cases} u_v^2/2g \ ; \ u_v > 0 \\ 0 \ ; \ u_v \leq 0 \end{cases} \tag{15}$$

where $(\hat{R},\hat{t})$ and $(\hat{R},\hat{t})$ are related according to Equations (5) and (6), $t^{(1)}_{max}$ is the R-dependent time defined in Section 2.3, $\overline{C}$ is a characteristic wavespeed in ground material at a given range (e.g., the wavespeed found when $U^{(1)}_{max}$ is obtained from Equation (7)) and

$$\hat{r}^2 = \hat{R}^2 + \hat{d}^2 \tag{16}$$

Equation (13) sets the time at which the direct-induced field is to be examined at any given range R and depth d, namely, the time of arrival of the direct wave at range R along the ground surface, plus the time of travel of a release wave from the surface to depth d. For that time and depth, the vertical velocity resulting from complete vertical stress relief is

superposed in Equation (14) on the downward vertical component of velocity left in the wake of the direct pulse. Velocities computed from Equation (14) have the greater-than-zero values $U_{max}^{(1)}$ (Equation (7)) when d=0, must fall to zero at some finite depth d > 0, and should do so monotonically. Hence d will be smaller than $u_v^s/2g$ when d is zero, and greater than $u_v^s/2g$ at some finite depth. For some finite value of d, namely d_c, Equation (15) must therefore be satisfied. Below the depth d_c, particles starting on ballistic trajectories with the vertical velocities prescribed by Equation (14) will not rise as high as the original ground surface, and therefore cannot be ejected from the crater. Furthermore, ejection of such material by plastic flow over the rim of the crater we find an unlikely process, and not just because deviations of stress from static equilibrium distributions decrease too rapidly (Section 1.3.8). Such a process would also require either that (a) kinetic energy of horizontal motion be converted efficiently to kinetic energy of vertical motion, or (b) kinetic energy be transferred from slower-moving to faster-moving material. However, the horizontal component of particle velocity does differ from zero as a general rule, and a radial redistribution of material will take place at depth d_c that can alter the shape of the crater; the volume of the crater, with which we are primarily concerned at present, would not be affected in the process.

As in the case of material at the ground surface, the kinetic energy of all material on the crater region should be considerably overestimated, since no energy is allowed to leave the ground in the spherical field from which σ_φ and u_r are taken. Hence, Equations (13) through (16) should provide values of d_c that bound the crater depth. Application of those equations has not yet been made.

2.7 Surface Waves; Velocity Amplitudes from Identical Compression Sources on an Elastic Half-Space and in an Infinite Elastic Medium

So far, no one seems to have suggested that nuclear craters are dug by Rayleigh waves, but if all else fails ... In any case, if only to assess the credibility of results like those presented above, it is necessary to examine the idea that the process of crater formation is intrinsically "two-dimensional", and cannot be simulated or bounded by more elementary motions. To explore that idea rigorously seems impossible. Instead, we compare exact ground-surface velocities for a specific problem of motion to approximate velocities obtained from a spherically symmetric field by the methods of Section 2.3.

Fortunately, the limited set of exactly soluble ground-motion problems contains at least one relevant member, namely, motion induced in a linear elastic half-space by a spherically symmetric source. A primitive source of ground motion of that kind was provided by the variation of velocity with range calculated at a time of 34 ms for a tamped 2-KT burst in salt. For use in the elastic-medium calculations discussed here, a point source was constructed that would reproduce in an infinite elastic medium the velocity-range data cited. The medium itself, an elastic approximation to salt, was assigned longitudinal and shear wave speeds of 14.5 ft/ms and 8.4 ft/ms, respectively, and its Poisson's ratio (the only property of real importance) was therefore equal to .25. Since the source so defined produces a spherically-symmetric field in an infinite medium, it generates only longitudinal waves. However, mode conversion at the surface of a half-space gives rise to shear waves as well, and to the combinations of the two basic wave-types that comprise Rayleigh waves.

Motion of the free surface of an elastic medium, driven by a source just below that surface, affords a stringent test of the present scheme for setting an upper bound on ground-surface velocities. In the first place, Rayleigh waves, which contribute strongly to such motion, have no counterpart in either uniaxial or spherically-symmetric fields - the very fields that we have used exclusively above to set bounds on vertical ground-surface velocities. Secondly, the characteristic decay of Rayleigh-wave amplitude with depth, which amounts to a factor of 1/e for each depth interval of about .4 wavelengths, bespeaks a concentration of energy at the ground surface that we have neglected entirely. Hence, if any inherently two-dimensional mechanism exists that would defeat our attempt to bound near-surface vertical velocities, Rayleigh waves would appear to embody that mechanism. Moreover, converting the fully-developed field from a tamped 1-KT burst to an elastic point-source, enables surface-wave formation to proceed from zero range outward, but does not enhance (or even alter) the infinite-medium elastic field produced by that source. The problem chosen for study also clearly addresses the question of ground-motion amplitude as it most directly concerns us, namely, at the surface of a half-space, and near a localized source of disturbance.

An exact expression for the disturbance radiated by a point-source in a medium comprised of two linear half-spaces, was derived by Sommerfeld,[16] and perhaps earlier by other authors. Explicit formulas for the field generated by a point-source of compressional waves below the free surface of an elastic half-space, are given in a more recent publication,[17] with the field expressed in the frequency domain. We have generated equivalent expressions in the time domain, and have evaluated those expressions for the case in which the compressional-wave source described

above is embedded in our elastic version of salt at a depth, in feet, of $9.3(1000\alpha W_{MT})^{\frac{1}{3}}$ (Section 2.3). As a function of range along the ground surface, the peak vertical velocities so derived are plotted in Figure 9, together with corresponding data obtained for a spherical elastic field by the procedure summarized in Equation (7). As represented in Figure 9, the source of motion has a strength appropriate to a 1-MT surface burst in which 8% of the yield is coupled to the ground.

The relatively slow decay of amplitude of the half-space solution in Figure 9 is presumably due to cylindrical divergence of outgoing Rayleigh waves, as opposed to near-field spherical divergence of waves in the corresponding infinite medium. As a result, although the spherical field yields much higher peak vertical velocities near ground zero, peak velocities from the half-space field begin to exceed those obtained from the spherical field at a range of 440 feet. At 640 ft of range, the half-space velocity is twice that deduced from the spherical field, while the difference amounts to a factor of 4.2 at a range of 1000 ft. One might therefore conclude that on the outer portions of the expected crater region, our "upper-bound" velocities are lower than the maximum vertical velocities they supposedly bound. However, while the data at hand do not help to establish the velocities of Figures 1 through 4 as upper bounds, neither can one conclude that the reverse is true, since: (a) In the tamped-burst calculation from which we obtained the source of elastic motion, the salt medium failed in shear out to a range of 1000 ft, and even beyond. (b) After a short time, only vapor is bound near the ground surface out to a range of 134 ft, and severe cracking takes place in the wake of the outgoing compression wave out to a range of several hundred feet. It is therefore quite unlikely that a process akin to Rayleigh wave formation can start within a few hundred feet of ground zero, to

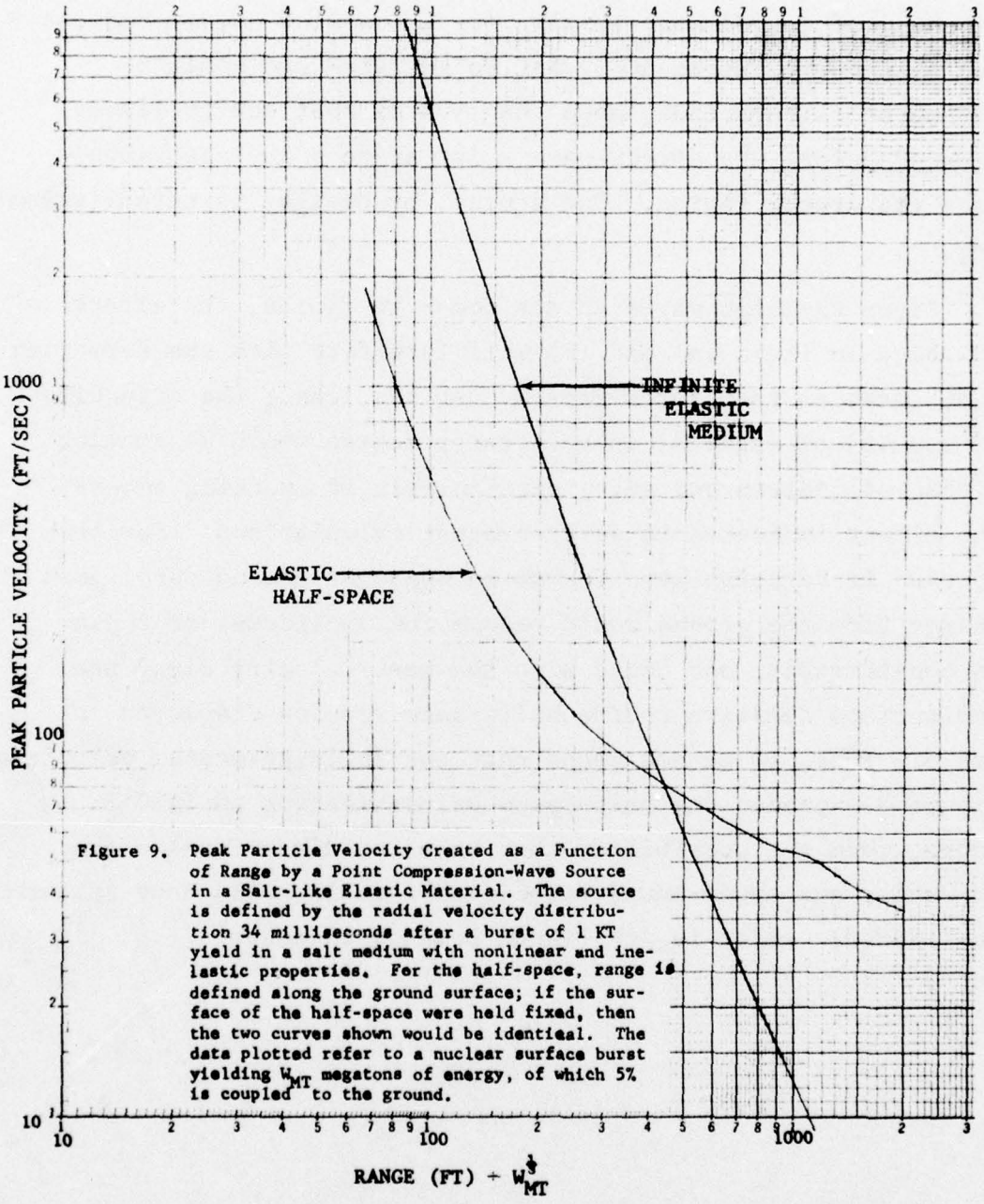

Figure 9. Peak Particle Velocity Created as a Function of Range by a Point Compression-Wave Source in a Salt-Like Elastic Material. The source is defined by the radial velocity distribution 34 milliseconds after a burst of 1 KT yield in a salt medium with nonlinear and inelastic properties. For the half-space, range is defined along the ground surface; if the surface of the half-space were held fixed, then the two curves shown would be identical. The data plotted refer to a nuclear surface burst yielding W_{MT} megatons of energy, of which 5% is coupled to the ground.

say nothing of ground zero itself. (c) All coupled energy remains in the half-space, while according to surface- and shallow-buried-burst calculations, more than 90% of that energy leaves the ground before the direct wave - let alone a Rayleigh wave - crosses the crater region. The source, by design, is unrealistically strong.

Since Rayleigh waves do not occur in fluids, the effects noted above in items (a) and (b) will interfere with the formation of such waves on the crater region. At the least, the effective shear modulus of material in the crater region would be smaller than that of undisturbed salt, particularly if cracking occurs to the extent indicated in surface-burst calculations. Furthermore, even if Rayleigh-wave formation began at ground zero, loss of energy from the ground would reduce the amplitudes of those waves considerably, and hence also the peak velocity along the ground surface relative to the half-space results displayed in Figure 9. Thus, if we had found that the infinite-medium velocities of Figure 9 exceeded the half-space velocities out to 1000 ft of range, then the possibility that some two-dimensional effect might render our upper-bound velocities invalid would have appeared slight indeed. As it is, the issue remains in doubt.

SECTION 3
CLOSING COMMENTS

Work remains to be done to determine the non-scalable factor (already known to be at least as large as 1.7) by which overpressure effects can influence the dimensions of craters formed by nuclear surface bursts. Also, our upper bound to crater depth is not well-defined at present. Nevertheless, the outlines of a crater whose dimensions represent a useful upper bound for surface bursts are discernable from the work reported here. At the maximum coupled-energy-fraction associated with Source 3 (8%), and a yield of 1 MT, the radius of that crater ranges from 990 ft for tuff to 1230 ft for granite. However, within a few microseconds after detonation half the coupled energy of 8% is found above the original ground-surface plane; our upper-bound crater radii run from 810 ft in tuff to 1000 ft in granite when the coupled-energy-fraction is 4%. Canonical crater radii cover the range 930-1060 ft, the lesser radius corresponding to a volume of 100 ft^3/ton and the greater to 150 ft^3/ton. For a crater 1100 ft in radius, we find typical upper-bound depths of 10.5, 19, 56, and 306 ft at ranges of 1000, 900, 750 and 500 feet respectively. The depths cited become increasingly loose upper bounds at smaller and smaller ranges; in fact, for ranges smaller than 500 ft, it becomes pointless to compute them. A procedure for establishing more realistic upper-bound depths has been devised, but remains to be applied.

3.1 Looseness of the Upper-Bound Crater Dimensions Reported Here

For the moment let us ignore the effects on crater size of the interaction of ejecta fragments with fireball gases; that kind of interaction, which leads to a reduction of crater size, has not been included in the upper-bound crater dimensions just quoted. Even so, the ranges noted, including the bounds on crater radius, could be overestimated by a factor as great as 2. We arrive at

that factor by recalling that (a) according to best present estimates, derived from surface-burst calculations, over 90% of the maximum energy coupled in a nuclear surface burst is transported to the fireball region in a time quite short compared to the time of crater formation, (b) all coupled energy has been assumed to remain below the ground surface in computing the upward velocities of surface material at the ranges cited, and (c) the rules of simple scaling apply with little error to the velocity field from which those ranges were deduced.

3.2 The Contribution of Plastic Flow to Crater Dimensions

The contribution of plastic flow to crater formation is included in the upper-bound dimensions quoted, but only to the extent that such flow would occur if the ground surface remained rigid after energy coupling; in that case a spherically symmetric field would develop about the burst point. On the other hand, plastic flow along the crater bottom, up the wall of the crater, and over the crater lip ("tangential plastic flow"), is a mechanism that we have explicitly excluded from our upper-bound estimates. If most of the crater volume were accounted for by tangential plastic flow, then our "upper-bound" velocities would not, in fact, be upper bounds. However, by definition, ejecta craters do not form primarily by tangential plastic flow, or by any other plastic flow process. Strictly speaking, consideration of plastic flow effects therefore lies outside the original scope of the study. Nevertheless, the possibility of crater formation by plastic flow has been explored here to some extent, with the following results: (a) We find no reason to believe that tangential plastic flow accounts for more than a minor fraction of the crater volume for materials whose von Mises limits of strength exceed 100-200 psi, and several reasons for believing that it

does not. (b) The total contribution of plastic flow to the crater volume can be appreciable, but only for materials with little strength. In particular, we find that for a coupled-energy-fraction (α) of .08, a canonical crater can result from plastic flow alone only in materials whose von Mises limits of strength are less by some undetermined amount than .42 ksi (.19 ksi if α=.04); plastic flow can account for 10% of the crater volume only when the von Mises limit is smaller (perhaps much smaller) than 6.2 ksi (2.8 ksi if α=.04). (c) In the crater region, plastic flow is associated mainly with motion directed radially outward from the shot point within .1 sec after a 1-MT burst, and not with tangential motion that takes place over a second or more.

Thus, we are left with upper-bound crater radii that exceed the canonical radius by only about 10%, and that could already be too large by as much as a factor of 2 even without taking account of ejecta-fireball interactions. We now turn to the effects of such interactions.

3.3 Ejecta-Fireball Interactions and Crater Size

While the influence of fireball gases on ejecta fragments has yet to be included in our crater-size bounds, some idea of the potential change in crater dimensions can be given now. The canonical overpressure has been applied to the ground surface in almost all nuclear surface burst calculations, and the impulse delivered by that overpressure to a unit area of the ground surface therefore comprises essential data for such an assessment. At times of .1, .2, .3 and 1 sec after arrival of the direct pulse, the overpressure-impulse per unit area of ground surface has the following values for a 1-MT surface burst, in units of bar-seconds: 2.0, 2.9, 3.6, and 5.5 at a range of 1000 feet; 2.3, 3.4, 4.0 and 6.0 at a range of 750 feet; and 3.8, 5.0, 5.7 and 7.8 at a range of 500 feet.

Cratering calculations are generally run to times of at least 1 sec after detonation. Under the pressure exerted by fireball gases during the second following arrival of the direct pulse, we estimate that craters in granite, limestone, salt and tuff would have final radii considerably smaller than 905, 715, 815 and 845 ft, respectively, even for a coupled-energy-fraction of .08; with 4% of the yield coupled to the ground the corresponding radii are 705, 560, 640 and 600 ft. Those radii are obtained when (a) the crater depth at each range is equated to the height to which a particle would rise, given the bounding vertical velocity obtained from calculations of tamped bursts, (b) all material is assumed to rise at the bounding vertical velocity, from the ground surface down to the exaggerated depth of the crater floor obtained from condition (a), and (c) the edge of the crater is defined by the requirement that downward impulse from fireball gases equal the upward vertical momentum implied by conditions (a) and (b).

Condition (a) leads to an overly-rapid increase in crater depth with decreasing range, and a proportional too-rapid decrease in the downward velocity increment induced by overpressure. In particular, the crater depth implied by condition (a) is proportional to the square of the vertical velocity, itself equated to an upper-bound value for surface material. The total vertical momentum to be offset by the impulse delivered to the ground by fireball gases is then proportional to the cube of the vertical velocity bound. Nevertheless, at the diminished crater radii noted above, the overpressure impulse per unit area sufficed to cancel the vertical momentum in columns of material about 54 feet high, moving upward at about 58 feet per second. Using more realistic bounds on crater depth and vertical velocity it would not be surprising to find that when the canonical overpressure is imposed on the

ground surface, calculated ejecta craters cannot be larger in radius than 500 feet.

Computed fields of surface-burst-induced motion often develop extensive and persistent regions of cracked material, especially on the crater region. In fields of cracked material, the canonical overpressure has acted to suppress the formation of ejecta to a greater degree than is indicated by the preliminary estimates just presented. Thus, rapid equilibration of pressure around ejecta fragments, which appears more realistic than no equilibration at all, will enlarge by a considerable factor both the ejecta mass and crater volume in any such field. In any case, it should be borne in mind that there is little or no evidence that the canonical overpressure is even qualitatively correct on the crater region; the possibility - even the likelihood - of its being in substantial error on that region is not generally disputed. In that regard, we note that several mechanisms are present among the phenomena occurring at the fireball-ground interface that could relieve the ground surface of gas pressure altogether for a second or so. Even on computational fields of motion where extensive cracking does not take place, the downward push of overpressure would then be eliminated. For the media considered here, that push contributes a downward velocity of only a few feet per second to surface material at a range of 100 ft from a 1 MT burst. For more readily compactible material, like that found at the surface of the U-2 medium, near-surface material acquires substantial downward velocities (20-40 ft/sec) prior to arrival of the direct pulse. Moreover, relief of direct-wave stresses takes place by both upward and downward motion at the top and bottom surfaces, respectively, of a thin layer of material, compacted by airblast loading, through which the direct wave runs at and near the ground surface.

3.4 Conditions for Forming Plastic-Flow Craters, Ejecta Craters and Compaction Craters

The results presented above, though incomplete, have important implications for present computational models of crater formation. Basic to deductions that will now be made from those results is the assumption that crater volumes of about 100-150 ft^3/MT result from nuclear surface bursts.

We note first that the conditions for creating ejecta craters can now be specified, at least semi-quantitatively. In particular, we find that compaction, and ejection of free-flying material, are the principal processes by which craters form in any medium whose von Mises limit of strength exceeds a certain limiting value. That value is no greater than 1 ksi, and probably much smaller; at 1 ksi a crater volume of 50 ft^3 per ton of yield can be produced by plastic flow if 8% of the yield is coupled to the ground and remains at all times below the ground surface-plane. We recognize, of course, that in the limit of vanishingly small angle of internal friction the von Mises limit will not determine the contribution to crater volume from plastic flow. However, even in a material with a von Mises limit of 500 bars (7.25 ksi), a decrease of the angle of internal friction to $9\frac{1}{2}^\circ$, with zero cohesion, caused the plastic-flow volume to increase by a factor of only 1.3. Among scores of geologic materials for which state-of-the-art strength data are readily at hand at ATI, only one or two have internal friction angles smaller than $9\frac{1}{2}^\circ$ - and then only slightly smaller. Moreover, the smallest angles of internal friction are generally found in materials with the lowest von Mises limits (100 to 400 psi), in which plastic flow is influenced least by the angle of internal friction. With regard to plastic flow, we therefore conclude that at the great majority of continental sites (excluding lakes and major

rivers) nuclear surface bursts in the megaton range would produce ejecta and/or compaction craters.

While we have given relatively little attention to the influence of air-void-fraction on crater volume, it seems clear that for air-void fractions at least as large as 3%, and probably a good deal larger, compaction cannot account for as much as 25% of the canonical crater volume. Again, as in describing the shear strength of a material by its von Mises limit, we recognize that inelastic volume changes are not described completely by a single number (the air-void-fraction). A more complete description would include a relation between mean stress and the irreversible volume strain produced by that stress. However, among the geologic materials known to us with air-void-fractions of a few percent or less, removal of air voids from even the most readily compactable substances would not account for a quarter of the volume of a standard crater in a nuclear surface burst. In fact, only in thin layers of topsoil do air-void-fractions exceed 3% at continental sites of primary defense interest. Hence, we conclude that nuclear surface bursts would produce ejecta craters at most of those sites.

Craters can now be divided into three groups corresponding to the fundamental cratering mechanisms of plastic flow, ejecta production, and compaction, based simply on the von Mises limit and air-void-fraction of a given ground medium. Specifically, craters will form mainly by means of ejecta production for materials with von Mises limits as low as 1 ksi (and probably much less), and air-void-fractions as great as 3% (and probably considerably more). Thus, we find that plastic-flow craters are produced in quasi-fluid media ($Y_{VM} < 1$ ksi) by nuclear surface bursts, ejecta craters in solid media ($Y_{VM} > 1$ ksi;

air-void-fraction less than 3%), and compaction craters on dry, porous media (air-void-fraction greater than 3%).

3.5 Sources of Error in Present Computations of Surface-Burst Craters

To the extent that the strengths of geologic materials are known, we find (for reasons discussed in detail above) that present computational models will produce craters of expected size either not at all, or mainly by the mechanism of ejecta formation. Further, most of the contribution of plastic flow to crater volume will be made early in the period of crater formation, and not by slow horizontal flow over a period of seconds. With those results in mind, we now ask why computed craters are so much smaller than is consistent with experimentally-based expectations.

A partial answer can be given to the question posed: When extensive cracking occurs on the region of computation, as in the case of granite, overpressure will inhibit ejecta formation and reduce crater volumes by factors at least as large as four, but whose maximum remains to be determined. Nevertheless, the results discussed above indicate that the computed volumes of ejecta craters produced by Source 3 are not likely to exceed 30 ft^3 per ton of yield, even if overpressures are reduced to zero. Such a volume, though somewhat lower than might generally be expected, would be credible for a surface burst on granite, and would therefore provide a unique and hence sorely needed point of correspondence between computed and actual craters. However, the ability to compute credible crater dimensions for nuclear surface bursts would even then be limited to hard-rock media. Furthermore, although little is known about the pressure of fireball gases near the ground surface in the early stages of a nuclear surface burst, there is no positive justification at present for reducing that pressure to zero as ejecta leave the crater.

With regard to the one other principal direction of hopeful speculation, it is possible that for surface bursts on quasi-fluids (i.e., materials with strengths < 100 psi), computed crater volumes will approach the values desired. Unfortunately, the data now available on the strengths of geologic solids tend to reduce quasi-fluid behavior to the status of a singular limiting case. While exploration of that limit may help to explain how craters form on Pacific atolls, there is no convincing evidence - and no direct evidence at all - to show that the media found at continental sites turn into quasi-fluids during crater formation.

The production of craters by ejecta formation (and by plastic flow as well) would almost certainly be enhanced by increasing the fraction α of the yield coupled to the ground, if the spatial distribution of coupled energy were not altered greatly in the process. In the absence of strong overpressure effects, calculated crater volumes are nearly proportional to α, and uncertainty in α therefore remains a potential source of significant error in predicting crater dimensions. In the case of ejecta craters in hard rocks, where computed and expected volumes may well lie within a factor of 2 or 3 of each other (if overpressure effects are negligible), an increase of 50% in α would be appreciable. On the other hand, more accurate coupling calculations could show that presently accepted values of α are too large.

While little present justification exists for assuming that geologic materials are quasi-fluids during crater formation, the issue of material properties is by no means a dead one. It is practically a truism that the results of cratering calculations, and indeed of all calculations of ground motion, depend heavily on the constitutive equations used to represent geologic materials. The suspicion that present constitutive relations for soils and rocks may contain fundamental defects, has been growing for

several years, and one need not look to phenomena as complex as crater formation to find evidence therefor. In particular, calculations of motion from tamped bursts almost invariably show a pronounced and rather abrupt drop in the rate of decay of peak velocity with range where shear failure ceases; beyond that range the energy carried by a computed outgoing pulse is no longer dissipated in shear. Of course, in a non-ideal world, abrupt changes tend to become diffuse. Even so, however, measurements of particle velocity in many tamped explosions give little indication that, as peak stress levels drop in an outgoing pulse, a range interval is reached over which a pronounced decrease takes place in the rate of decay of peak particle velocity. The fact that experimental data consistently exhibit little or no evidence of such a transition casts doubt on the validity of one of the basic building blocks of present constitutive models, namely, the equations that describe the behavior of material in states of shear failure. Furthermore, the difficulty is not easily resolved by varying parameters of the present equations; within the framework of those equations, the qualitative feature of calculated pulse decay cited can apparently only be eliminated by gross and arbitrary changes in material strengths relative to those measured. Hence, the mathematical framework into which data from strength tests are presently incorporated, is itself suspect. For the soft-rock media found at most sites of interest, a substantial part of the sought-for factor of 50 in crater volume might be found by resolving a basic question: In what ways are present mathematical descriptions of shear failure inadequate?

REFERENCES

1. Results presented by several organizations at the Cratering Working Group Meeting of 28 May, 1975

2. Trulio, J.G., "Calculations of Cratering, Ejecta and Dust Lofting", DASA 2507, p. 27 (August, 1970)

3. Roddy, D., Boyce, J., Colton, G., and Dial, A., "Meteor Crater, Arizona, rim drilling with thickness, structural uplift, diameter, depth, volume and mass-balance calculations", Proc. Lunar Sci. Conf. (6th) (Pergamon Press, 1975)

4. Brode, H., Letter to M. Baron (31 October 1966)

5. Trulio, J., Ramshaw, J., Glenn, L. and Carr, W., "Calculations of Device-Air-Ground Interaction in a Scaled Smallboy Burst," DNA 3405F (report unpublished).

6. Layson, W., et al, "Nuclear Surface Burst Debris and System Vulnerability DASA 69-03041 (report unpublished).

7. Trulio, J. and Glenn, L., "Pressure Equilibration Around Ejecta in a Nuclear Surface Burst", DASA 2457 (June 1970)

8. Reference 2, p. 22-24

9. Trulio, J. and Perl, N., "Calculations in Support of the Diamond Dust and Diamond Mine Events", DNA 3268F, p. 25-27 (12 February 1974)

10. Trulio, J., Ialongo, G., McDonald, J., and Srinivasa, D., "Overdrive Calculations Related to Nuclear Explosions", DNA 3542F, p. 29, 48, 49 (18 June 1975)

11. Schuster, S., and Isenberg, J., "Free Field Ground Motion for Beneficial Facility Siting", SAMSO-TR-70-88 (June 30, 1970)

12. Brode, H.; conversation

13. Knowles, C.; conversation

14. Reference 2, Figures 22, 23

15. Trulio, J. and Perl N., "Decoupling with Explosively-Formed Cavities", ATR-41-75-2 (Final Report for Contract No. DNA 001-74-C-0238; to be published)

16. Sommerfeld, A., "Partial Differential Equations in Physics", p. 237-257 (Academic Press, 1949)

17. Ewing, W., Jardetzky, W., and Press, F., "Elastic Waves in Layered Media", p. 43, 44 (McGraw-Hill, 1957)

DISTRIBUTION LIST

DEPARTMENT OF DEFENSE

Director
Defense Advanced Rsch. Proj. Agency
ATTN: NMRO
ATTN: Technical Library

Director
Defense Civil Preparedness Agency
Assistant Director for Research
ATTN: Admin. Officer

Defense Documentation Center
Cameron Station
12 cy ATTN: TC

Director
Defense Nuclear Agency
ATTN: TISI, Archives
ATTN: DDST
2 cy ATTN: SPSS
3 cy ATTN: TITL, Tech. Library

Commander
Field Command
Defense Nuclear Agency
ATTN: FCPR

Director
Interservice Nuclear Weapons School
ATTN: Document Control

Director
Joint Strat. Tgt. Planning Staff, JCS
ATTN: STINFO Library

Chief
Livermore Division Fld. Command, DNA
ATTN: FCPRL

Under Secretary of Def. for Rsch. & Engrg.
ATTN: S&SS (OS)

DEPARTMENT OF THE ARMY

Director
BMD Advanced Tech. Ctr.
ATTN: 1CRDABH-X
ATTN: CRDABH-S

Dep. Chief of Staff for Rsch. Dev. & Acq.
ATTN: Technical Library

Commander
Harry Diamond Laboratories
ATTN: DRXDO-TI, Tech. Library
ATTN: DRXDO-NP

Director
U.S. Army Ballistic Research Labs.
ATTN: DRXBR-X, Julius J. Meszaros

Director
U.S. Army Engr. Waterways Exper. Sta.
ATTN: Guy Jackson
ATTN: Technical Library

DEPARTMENT OF THE ARMY (Continued)

Commander
U.S. Army Materiel Dev. & Readiness Cmd.
ATTN: Technical Library

Commander
U.S. Army Nuclear Agency
ATTN: Tech. Library

DEPARTMENT OF THE NAVY

Officer-In-Charge
Naval Surface Weapons Center
ATTN: Code WA501, Navy Nuc. Prgms. Off.

DEPARTMENT OF THE AIR FORCE

AF Geophysics Laboratory, AFSC
ATTN: SUOL, Rsch. Library

AF Weapons Laboratory, AFSC
ATTN: DEP, Jimmie L. Bratton
ATTN: DES-C, Robert Henny
ATTN: SUL

Headquarters, USAF/RD
ATTN: RDQSM

DEPARTMENT OF ENERGY

University of California
Lawrence Livermore Laboratory
ATTN: Tech. Info. Dept., L-3

Los Alamos Scientific Laboratory
ATTN: Doc. Control for Reports Library

Sandia Laboratories
Livermore Laboratory
ATTN: Doc. Control for Tech. Library

Sandia Laboratories
ATTN: Doc. Control for 3141,
Sandia Rpt. Coll.

DEPARTMENT OF DEFENSE CONTRACTORS

Aerospace Corporation
ATTN: Tech. Info. Services

Agbabian Associates
ATTN: M. Agbabian

Applied Theory, Inc.
ATTN: Raymond W. Latham
ATTN: Neil K. Perl
2 cy ATTN: John G. Trulio

Battelle Memorial Institute
ATTN: Technical Library

The BDM Corporation
ATTN: Technical Library

DEPARTMENT OF DEFENSE CONTRACTORS (Continued)

The Boeing Company
ATTN: Aerospace Library
ATTN: R. M. Schmidt

California Research & Technology, Inc.
ATTN: Sheldon Shuster
ATTN: Ken Kreyenhagen
ATTN: Technical Library

Civil/Nuclear Systems Corp.
ATTN: Robert Crawford

University of Dayton
ATTN: Hallock F. Swift

University of Denver
Colorado Seminary
Denver Research Institute
ATTN: Sec. Officer for J. Wisotski

General Electric Company
TEMPO-Center for Advanced Studies
ATTN: DASIAC

Kaman AviDyne
Division of Kaman Sciences Corp.
ATTN: E. S. Criscione
ATTN: Technical Library

Kaman Sciences Corporation
ATTN: Library

Lockheed Missiles & Space Co., Inc.
ATTN: Technical Library

McDonnell Douglas Corporation
ATTN: Robert W. Halprin

Merritt CASES, Incorporated
ATTN: J. L. Merritt
ATTN: Technical Library

Nathan M. Newmark Consulting Engineering Services
University of Illinois
ATTN: Nathan M. Newmark

Science Applications, Inc.
ATTN: Technical Library

DEPARTMENT OF DEFENSE CONTRACTORS (Continued)

Physics International Company
ATTN: Doc. Control for Dennis Orphal
ATTN: Doc. Control for Fred M. Sauer
ATTN: Doc. Control for Tech. Library
ATTN: Doc. Control for Robert Swift

R & D Associates
ATTN: Robert Port
ATTN: Jerry Carpenter
ATTN: Henry Cooper
ATTN: Cyrus P. Knowles
ATTN: Technical Library

Science Applications, Inc.
ATTN: David Bernstein
ATTN: D. E. Maxwell

SRI International
ATTN: Burt R. Gasten
ATTN: George R. Abrahamson

Systems, Science and Software, Inc.
ATTN: Technical Library

Terra Tek, Inc.
ATTN: Sidney Green
ATTN: Technical Library

TRW Defense & Space Sys. Group
ATTN: Tech. Info. Center/S-1930

TRW Defense & Space Sys. Group
San Bernardino Operations
ATTN: E. Y. Wong, 527/712

The Eric H. Wang Civil Engineering Rsch. Fac.
University Station
ATTN: Neal Baum

Weidlinger Assoc. Consulting Engineers
ATTN: Melvin L. Baron
ATTN: J. W. Wright

Weidlinger Assoc. Consulting Engineers
ATTN: J. Isenberg